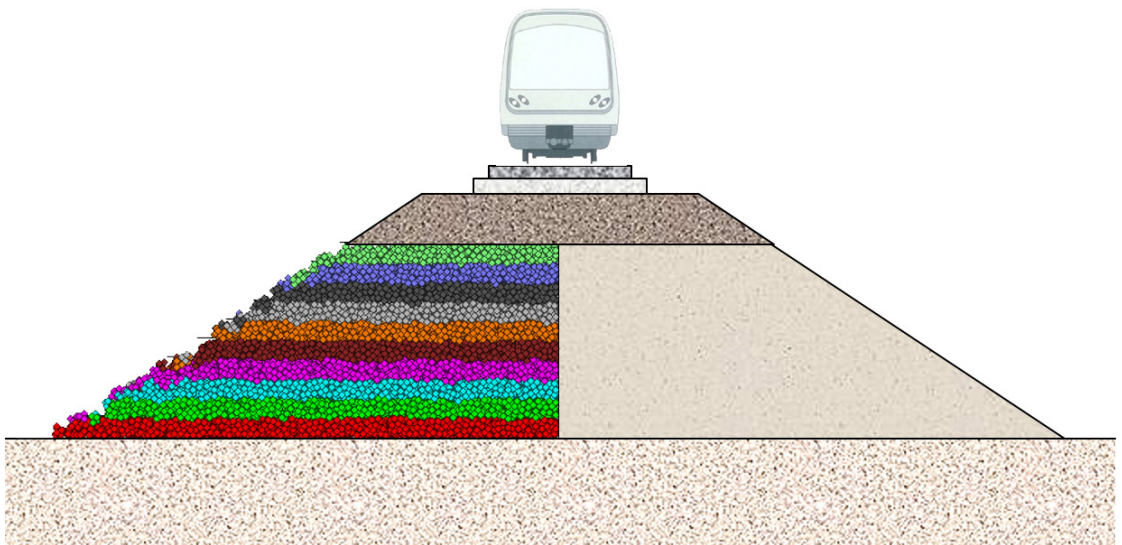


Doctoral Thesis in Transport Infrastructures

DEM Modelling of Unbound Granular Materials for Transport Infrastructures

On soil fabric and rockfill embankments

RICARDO DE FRÍAS LÓPEZ



DEM Modelling of Unbound Granular Materials for Transport Infrastructures

**On soil fabric and rockfill
embankments**

Ricardo de Frías López

Doctoral Thesis, 2020
KTH Royal Institute of Technology
School of Architecture and the Built Environment
Department of Civil and Architectural Engineering
Soil and Rock Mechanics Division
SE-100 44, Stockholm, Sweden

TRITA-ABE-DLT-205
ISBN 978-91-7873-509-9

© Ricardo de Frias Lopez, 2020

Akademisk avhandling som med tillstånd av KTH i Stockholm framlägges till offentlig granskning för avläggande av teknologie doktorsexamen tisdagen den 18 augusti 2020 kl. 13:00 i Kollegiesalen, KTH, Brinellvägen 8, Stockholm.

Abstract

Unbound granular materials (UGM) are widely used as load-bearing layers and for embankment construction within transport infrastructures. These play a significant role on operation and maintenance of transportation systems. However, pavement and railway engineering still today rely heavily on empirical models based on macroscopic observations. This approach results in limited knowledge on the fundamentals at particle scale dictating the macroscopic response of the material. In this sense, the discrete element method (DEM) presents a numerical alternative to study the behaviour of discrete systems with explicit consideration of processes at particulate level. Additionally, it allows obtaining information at particulate level in a way that cannot be matched by traditional laboratory testing. All of this, in turn, can result in greater micromechanical insight.

This thesis aims at contributing to the body of knowledge of the fundamentals of granular matter. UGM for transport infrastructures are studied by means of DEM in order to gain insight on their response under cyclic loading. Two main issues are considered: (1) soil fabric and its effect on the performance of coarse-fine mixtures and (2) modelling of high rockfill railway embankments. Among the main contributions of this research there is the establishing of a unified soil fabric classification system based exclusively on force transmission considerations that furthermore correlates with performance. In particular, fabrics characterized by a strong interaction between the coarse and fine fractions resulted in improved performance. A soil fabric type with a potential for instability was also identified. Regarding embankments, DEM modelling shows that traffic induced settlements accumulate on the top layers and therefore seem to be unaffected by embankment height above a certain value. A marked influence of degradation, even considering its nearly negligible magnitude, was observed, largely resulting in increased settlements.

Keywords

Discrete element method; granular materials; particle-scale behaviour; particle degradation; permanent deformation; resilient modulus; rockfill embankment; soil fabric.

Sammanfattning

Grus i form av krossat bergmaterial används i stor utsträckning som obundna bär- och förstärkningslager inom transportinfrastrukturen och spelar där en viktig roll för drift och underhåll. Områden såsom väg- och järnvägsbyggnad bygger emellertid fortfarande väsentligen på empiriskt baserade modeller till stor del grundlagda på makroskopiska observationer. Denna metod resulterar i begränsad kunskap om de fundamentala mekanismerna på partikelnivå (d.v.s. enskilda gruskorn) som styr det makroskopiska verkningssättet. Mot denna bakgrund utgör den s.k. diskreta elementmetoden (DEM) ett numeriskt alternativ för att studera verkningssätt hos diskreta system där man explicit beaktar mekanismerna på partikelnivå. Dessutom gör DEM det möjligt att få information på partikelnivå på ett sätt som inte kan matchas med traditionella laboratorieförsök. Allt detta kan i sin tur resultera i större mikromekanisk insikt.

Denna avhandling syftar till att bidra till kunskapen om grunderna för grusmaterialets verkningssätt. Obundna grusmaterial studeras med hjälp av DEM-modellering för att belysa verkningssätt under cyklisk belastning. Två huvudämnen beaktas: (1) skelettsstruktur och dess påverkan på verkningssättet för blandningar av fina och grova partiklar (2) DEM-modellering av höga järnvägsbankar. Bland de huvudsakliga forskningsbidragen är upprättande av ett enhetligt klassificeringssystem vad gäller skelettstruktur i grusmaterialet med enbart hänsynstagande till kraftöverföring som dessutom överensstämmer med grusmaterialets verkningssätt. I synnerhet observerades att skelettstrukturer som kännetecknas av en stark interaktion mellan grova och fina fraktioner resulterade i högre styvhet och mindre permanenta deformationer. Dessutom identifierades en typ av skelettstruktur med potential för instabilitet. Vad gäller järnvägsbankar visar DEM-modellering att trafikorsakade sättningar utvecklas främst på det översta lagret och därför inte påverkas av bankhöjden över ett visst värde. En väsentlig påverkan av nedbrytning, även med tanke på dess nästan försumbar storlek, observerades, vilket i hög grad resulterade i större sättningar.

Nyckelord

Diskreta elementmetoden; grusmaterial; verkningssätt på partikelnivå; nedbrytning; permanent deformation; styvhet; stenfylld bank; skelettstruktur.

Preface

The research leading to this doctoral thesis was mainly carried out during 2013-2020 at the department Civil and Architectural Engineering at the Royal Institute of Technology KTH in Stockholm, largely by the author as a part-time PhD student.

This work has been supervised by Professor Johan Silfwerbrand with the assistance of Professor Stefan Larsson. This thesis is the result of our combined efforts and both of them deserve my gratitude for their constant support, guidance and invaluable advice. Others to be acknowledge for their supervision and contributions on earlier stages of the research are, in no particular order, Professor Björn Birgisson, Associate Professor Denis Jelagin and Adjunt Professor Jonas Ekblad. Appreciation is also due to the following founding bodies for their financial support: Swedish Transport Administration, Development Fund of the Swedish Construction Industry SBUF and the Swedish research program Better Interaction in Geotechnics BIG. The support of Saitec Engineering is also acknowledged, and in particular of Björn Sennerfors, for allowing me to combine my work as a consultant with my doctoral studies. Finally, I would also like to thank my family and friends.

Stockholm, April 2020

Ricardo de Frías López

List of appended papers

This doctoral thesis is based upon the following published scientific articles (Papers I, II and IV) and conference publication (Paper III) together with a submitted manuscript for consideration as a scientific article (Paper V).

Publication I.

de Frias Lopez R, Silfwerbrand J, Jelagin D, Birgisson B.
Force transmission and soil fabric of binary granular mixtures.
Géotechnique. 2016;66(7): 578–583.
doi:10.1680/jgeot.14.P.199

Publication II.

de Frias Lopez R, Ekblad J, Silfwerbrand J.
Resilient properties of binary granular mixtures: A numerical investigation.
Computers and Geotechnics. 2016;76: 222–233.
doi:10.1016/j.compgeo.2016.03.002

Publication III.

de Frias Lopez R, Ekblad J, Silfwerbrand J.
A numerical study on the permanent deformation of gap-graded granular mixtures.
In: Pombo J (ed.) *Proceedings of the Third International Conference on Railway Technology: Research, Development and Maintenance*. Stirlingshire, UK: Civil-Comp Press; 2016.
doi:10.4203/ccp.110.15

Publication IV.

de Frias Lopez R, Larsson S, Silfwerbrand J.
A discrete element material model including particle degradation suitable for rockfill embankments.
Computers and Geotechnics. [Online] Elsevier Ltd; 2019;115.
Available from: doi:10.1016/j.compgeo.2019.103166

X

Publication V.

de Frias Lopez R, Larsson S, Silfwerbrand J.
Discrete element modelling of rockfill railway embankments.
Submitted to: *Granular Matter*. 2020.

In all publications, the author performed all the numerical simulations and analysis of the results. The original text was also written by the author. The co-authors helped with valuable comments and advice on both the research focus and the text structure, including a detailed review of the manuscripts.

Notations

Abbreviations

DEM	discrete element method
FEM	finite element method
FPL	frost protection layer
PDD	probability density distribution
PSD	particle size distribution
PSR	particle size ratio (D_c/D_f alternatively D_{\max}/D_{\min})
SMA	stone matrix asphalt
UGM	unbound granular materials
VTT	Technical Research Centre of Finland (Valtion Teknillinen Tutkimuskeskus)

Symbols

A	maximum possible value of failure ratio R_u
B	stress dependent material parameter
C_n	particle coordination number
$C_{n,\min}$	minimum coordination number governing particle splitting
D	sphere diameter
D_c, D_f	coarse and fine grain nominal size, respectively
D_{spc}	cylindrical specimen diameter
D_{\max}, D_{\min}	maximum and minimum grain size, respectively
E_c	contact elastic modulus
FC	percentage of fine grain content by weight
FC_{th}	threshold value of fines content
H_{spc}	cylindrical specimen height

H	nominal rockfill height
M_r	resilient modulus
N_c	number of interparticle contacts
N_{clp}	number of clump particles
N_{cl}^c	number of compaction cycles
$N_{p,c}, N_{p,f}$	number of coarse and fine particles, respectively
N_{sph}	number of spheres
R	sphere radius
R_1, R_2	radii of the two spheres in contact
R_u	failure ratio ($\sigma_d/\sigma_{d,u}$)
R^2	coefficient of determination
V	total volume of the specimen
$c-c, c-f, f-f$	coarse-to-coarse, coarse-to-fine and fine-to-fine interparticle contact-type networks, respectively
f_n, f_t	normal and tangential contact force, respectively
$f_{n,i}, f_{t,i}$	component i of normal and tangential components of the contact force, respectively
$\langle f_n \rangle$	average interparticle normal contact force for the whole system
$f_{n,f}$	normal contact force at fracture
k_n, k_s	particle normal and shear stiffness, respectively
$k_{n,wall}$	normal stiffness of the wall
\bar{k}_n	average normal stiffness of the particles
k_1, k_2, k_3	regression constants unique to each function and material
n_i	unit vector component i of normal contact force
n_o	initial porosity
p	mean normal stress ($\sigma_c + \sigma_d/3$)

p_o^t	target initial mean normal stress
q	deviator stress (σ_d)
t_i	unit vector component i of tangential contact force
t_{cont}^p	thickness of dumping container
v_{max}^c	maximum wall velocity during compaction
$v_{\text{max}}^{\text{PL}}$	maximum wall velocity during permanent loading
$v_{\text{max}}^{\text{TL}}$	maximum wall velocity during traffic loading
ε_a	axial strain
$\varepsilon_r, \varepsilon_p$	resilient and permanent components of the axial strain, respectively
$\dot{\varepsilon}_a$	axial strain rate
ε_v	volumetric strain
μ, μ_{wall}	particle and wall friction coefficient, respectively
μ_g	particle friction coefficient during generation
ρ	particle density
σ_c	confining stress under triaxial compression
σ_d	deviator stress under triaxial compression
$\sigma_{d,u}$	deviator stress at failure under triaxial compression
σ_{ij}	overall stress tensor component ij
σ_d^{c-c}	cumulative contribution to σ_d of the coarse-to-coarse contact network (coarse grain skeleton contribution)
σ_d^{c-f}	cumulative contribution to σ_d of the coarse-to-fine contact network (contribution by the interaction of both fractions)
σ_d^{f-f}	cumulative contribution to σ_d of the fine-to-fine contact network (fine grain skeleton contribution)
σ_n^c	maximum normal stress during compaction
σ_n^{PL}	maximum normal stress during permanent loading
σ_n^{TL}	maximum normal stress during traffic loading

Contents

Abstract	I
Sammanfattning	III
Preface	V
List of appended papers	VII
Notations	IX
1. Introduction	1
1.1 General background.....	1
1.2 Soil fabric and performance.....	4
1.2.1 Aims and scope	6
1.2.2 Limitations.....	7
1.3 Rockfill railway embankments	8
1.3.1 Aims and scope	11
1.3.2 Limitations.....	13
1.4 Outline of the thesis	14
2. Soil fabric and performance of binary mixtures	17
2.1 Soil fabric classification system	17
2.2 Particle size ratio.....	19
2.3 Numerical procedures	20
2.4 Results and discussions	23
2.4.1 Specimens	23
2.4.2 Soil fabric	25
2.4.3 Resilient modulus	28
2.4.4 Permanent deformation.....	30
2.4.5 Soil fabric and performance.....	33

3. High rockfill railway embankments	35
3.1 Particle degradation.....	35
3.1.1 Main processes, factors and significance.....	35
3.1.2 DEM implementation	36
3.2 Triaxial testing	39
3.2.1 Numerical procedures	39
3.2.2 Main results and discussion	42
3.3 Embankment modelling	47
3.3.1 Numerical procedure	47
3.3.2 Main results and discussion	51
4. Concluding remarks and further research	59
4.1 Concluding remarks.....	59
4.1.1 Soil fabric	59
4.1.2 Rockfill embankments	60
4.2 Further research	61
4.2.1 Material model and embankment generation	62
4.2.2 Embankment loading	63
References	65
Erratum (Publication IV).....	71
Appended papers	73

1. Introduction

1.1 General background

Aggregates are widely used as construction materials worldwide, both as unbound granular materials UGM and as part of other bound materials such as concrete or asphalt products. The yearly demand for aggregates across Europe¹ in 2017 was ca 2.7 billion tonnes, equivalent to 5 tonnes per capita and per year (1). Of these, over 40% were used in its unbound form (1). In Sweden, aggregates deliveries in 2017 accounted for almost 100 million tonnes (1,2) resulting in nearly 10 tonnes per capita, i.e. the fifth European country with the highest consumption per capita (1). Crushed rock extracted from quarries is the main type of aggregate used in construction, nearly 50% of aggregate sources at the European level (1) and 60% for the case of Sweden (2). In Europe, approximately 35% of aggregates are used for the construction of infrastructures such as roads and railways. However, when it comes to Sweden, 56% of aggregates were used for road construction alone in 2017 (2). The importance of UGM, mainly in its crushed rock form, in transport infrastructures cannot be overstated.

Unbound layers, in the form of load-bearing layers and fill material for embankment construction, constitute an integral part of pavement and railway systems. These layers play a significant role on performance and need for maintenance of these infrastructures. Among the most significant predictors and indicators of field performance of granular materials for transport infrastructures are the permanent strain response ε_p and the resilient modulus M_r . The former is a measurement of the permanent or irrecoverable part of settlements relative to layer thickness. The latter characterizes the material stiffness under cyclic loading and is associated with the recoverable or elastic part of the settlements. For cyclic triaxial loading under constant confinement stress, M_r is generally defined as the ratio of the repeated deviator stress σ_d to the recoverable or resilient part of the axial strain ε_r during unloading (3):

$$M_r = \frac{\sigma_d}{\varepsilon_r} \quad (1)$$

¹ European Union EU + European Free Trade Association EFTA

The complementary character of the above variables is illustrated in Figure 1. Their importance, together with the vast complexity of granular material behaviour, is indicated by the extensive literature review conducted by Lekarp et al. (4,5) concerning the numerous modelling techniques and influencing factors. This complex behaviour results in an inherent level of uncertainty on the mechanical response of granular layers, like the development of settlements due to traffic induced cyclic loading. This can be critical if, for example, design speeds are to be maintained on railway tracks, especially for the case of high-speed.

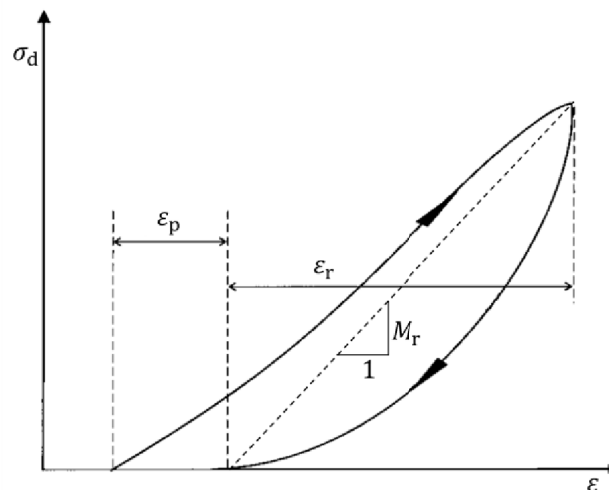


Figure 1. Stress-strain response of a granular material during one load cycle of cyclic triaxial loading.

The complex mechanical response of granular materials mainly stems from its discrete nature, where loads are transmitted through interparticle contacts. Processes like settlement accumulation develop progressively resulting from continuous particle rearrangement under a large number of loading cycles, generally accompanied by particle degradation that further facilitates this rearrangement. This results in a continuously evolving particle-to-particle contact network that defines the load-bearing skeleton of the assembly. In this sense, it is no wonder that conventional engineering modelling techniques that are based on assimilating the considered domain to a continuum, like the well-established finite element method FEM, result in limited success in capturing the fundamentals of granular materials and hence in predicting their long-term evolution in

performance. In fact, the inadequacy of regarding granular materials as a continuum was already recognized at the very foundations of the soil mechanics discipline by Terzaghi (6) and later highlighted by Rowe (7) when studying the dilatancy of sands. If this is true for granular materials in general, it can be recognized as even more relevant for unbound layers in infrastructures. For example, treating a railway ballast layer, which is relatively uniformly graded with grain sizes generally ranging from 30 to 60 mm and a layer thickness of approximately 300 mm, e.g. (8), as a continuum is a vast oversimplification given the relatively large grain sizes compared to the problem geometry. Therefore, it is no wonder that pavement and railway engineering still today rely heavily on empirical design methods or, in the best of cases, on mechanistic-empirical methods where the long-term behaviour is accommodated by an empirically-based performance function. Furthermore, all the above methods result in rather limited insight on the fundamentals of granular matter mainly due to:

- limitations in conducting comprehensive measurements at particle level for granular assemblies during laboratory testing
- difficulties in incorporating processes at particle level on the material model in an explicit manner in conventional semi-mechanistic methods based on a continuum domain approach

In these regards, the so-called discrete element method DEM does overcome the above limitations to a certain extent. DEM is a numerical method originally proposed by Cundall (9) for the analysis of rock-mechanics problems and later implemented to soils by Cundall & Strack (10). It has been intensively used during the last decade for the study of granular materials for pavement and railway applications, e.g. (11–14). It presents a powerful numerical tool to study the macroscopic behaviour of discrete systems with explicit consideration of internal processes at particulate level. Additionally, it allows obtaining information at particulate level in a way that cannot be matched by traditional laboratory testing. All of this, in turn, results in a much greater micromechanical insight into the fundamentals of granular matter. Nevertheless, DEM has its limitations. Among these, computational time is paramount. When large collections of particles are involved, modelling cyclic loading comes with great computational time demands. This limitation becomes aggravated with increasing numbers of load cycles and by including particle degradation in the material model, e.g. (11,15).

This thesis is aimed at contributing to the body of knowledge of the fundamentals of granular matter, specifically for the case of UGM for transport infrastructures. In order to achieve this, DEM modelling is used as the main tool to gain micromechanical insight into the mechanical response of the material under structural loading. Two different questions are considered. In the first part, comprising publications I-III, the soil fabric and its effect on performance are investigated, with a certain emphasis on base and sub-base unbound layers for flexible pavements as used in Sweden. This part can be considered of a more theoretical nature. In the second part, comprising publications IV and V and of a more applied nature, high rockfill railway embankments, with an emphasis on slab-track configurations, are studied using DEM. The influence of embankment height and different processes at particle level, like particle breakage, on the macroscopic mechanical response to cyclic loading induced by traffic is studied. This is something not attempted before due to computational time demands.

1.2 Soil fabric and performance

Numerous factors influence the permanent strain response and the resilient response of granular materials for transport infrastructures (4,5). Among these, the stress level is considered as the most significant external structural factor governing the resilient response of granular layers (4), which is also true for the development of permanent deformations in addition to the number of load applications (5). Regarding material or internal factors, particle size distribution PSD is one of the most influential properties affecting the force transmission and soil fabric of granular materials and consequently their performance. PSD or gradation is usually characterized by the gradation curve, obtained by sieve analysis. This is in fact one of the most commonly used material requirements in specifications for different applications of both UGM and stone-based bound materials for engineering purposes.

Unlike more continuously or densely graded granular mixtures, gap-graded mixtures are materials with gradations that contain none or very small amounts of aggregate sizes in the mid-range. This leads to two clearly differentiated fractions regarding grain sizes, namely the coarse and the fine, respectively. The PSD of these materials can therefore be characterized by nominal values representative of the coarse and fine grain sizes, D_c and D_f , respectively, and by the relative percentage by weight of fine particles content FC . These mixtures can be found in natural soils such as residual and colluvial soils and have attracted a certain degree of attention in the study of slope stability, e.g. (16–20). They are also used for

different engineering applications, such as fills for rockfill dams, or in some types of asphalt concrete mixtures, i.e. stone matrix asphalt SMA. In particular, SMA has shown improved rutting and wear resistance compared to more traditional dense-graded asphalt mixtures (21–23). Its application as railway ballast has also been investigated, suggesting performance advantages and lower degradation over more traditional uniform gradations (24). Figure 2 visually illustrates the difference between all the above mentioned types of mixtures.

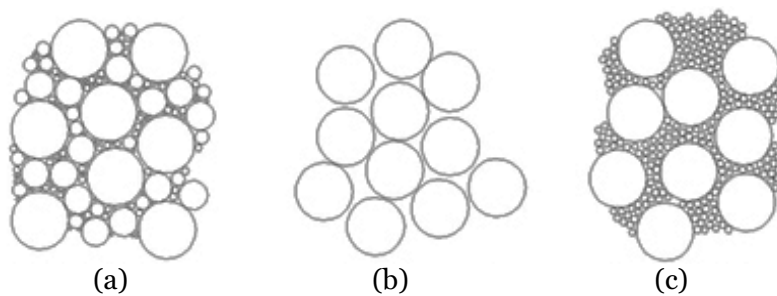


Figure 2. Illustration of typical aggregate gradations: (a) dense-graded, (b) uniformly graded and (c) gap-graded (25)

Gap-graded mixtures, also referred to as binary mixtures, represent the simplest case of soil fabric structure where the role of different grain size components on the mechanical response of the material can be studied. Compared to more general continuously graded mixtures, only two clearly distinct components exist. This leads to three interparticle contact-type networks alone: coarse-to-coarse *c-c*, coarse-to-fine *c-f* and fine-to-fine *f-f*. This allows for an easier conceptualisation and hence potentially improved understanding of the soil skeleton fabric. Furthermore, it could be hypothesized that, in general terms, any granular mixture may be conceptually simplified to either a uniformly graded material (e.g. clean railway ballast) or a binary mixture. Fine grains can be identified as those filling the gaps between coarser particles for low-to-intermediate fines content, whereas for higher fines content, coarse grains are floating in a matrix of finer grains. Different studies proposing methodologies to identify the coarse and fine components for pavement engineering applications exist (26,27).

Several authors have proposed soil fabric classification systems attempting to conceptually or qualitatively explain the role of the coarse and fine fractions on different aspects of the behaviour of gap-graded mixtures. Vallejo (28) proposed four cases explaining the shear strength development of rock-sand mixtures; Thevanayagam et al. (29) developed five classes concerning the liquefaction potential of sand-silt mixtures. In

both studies, the microscopic behaviour and fabric structure were inferred from the observed macroscopic response. Fabric cases were identified by the FC in relation to limit values based on empirical correlations with macroscopic response measurements and different macroscopic volumetric indexes. Difficulties in measuring responses at particulate level, like contact forces, imposed the above indirect approach to characterize granular fabrics, resulting in limited micromechanical insight.

1.2.1 Aims and scope

In this part of the thesis, the effect of soil fabric on performance of gap-graded materials is investigated. Firstly, a soil fabric classification system is quantitatively defined in terms of contact force transmission at particle level. This implies that fabrics are defined exclusively on micromechanical considerations regarding interparticle force transmission and without any regards whatsoever to macroscopic performance aspects. Secondly, the significance of the developed system on the resilient and permanent deformation response is assessed.

The main scope of this part of the thesis is the study of perfect binary mixtures of elastic spheres under axisymmetric stress conditions, i.e. triaxial loading, using DEM. Perfect binary mixtures of spheres represent the simplest expression of a non-uniformly graded material, allowing to study the significance of different grain size elements on the bearing skeleton of the mixture independently of particle shape, known to greatly influence performance (4,5). By establishing qualitative behavioural similarities with real UGM, results and conclusions could be partly extrapolated to real gap-graded granular mixtures. Furthermore, as already introduced above, any granular material may in principle be assimilated to a binary mixture, potentially allowing the extension of the results to continuously graded mixtures.

First, the relative contributions of the different interparticle contact-type networks to resist the applied deviator stress are determined. Results are used to define soil fabric cases to characterize the load-bearing mechanisms of gap-graded materials in accordance with existing classification systems, where the role of coarse and fine components are explicitly explained and quantified in terms of force transmission rather than inferred from the macroscopic response. This is covered by Publication I.

Subsequently, the effect of stress level on the resilient response of the mixtures is assessed. Behavioural similarities are established with existing empirically-based relations characterizing the stress dependency of the modulus for granular materials using different statistical tools. The stress dependency of the proposed fabric classification system is also determined and its correlation with resilient performance is analysed statistically. This is covered by Publication II.

Finally, the permanent strain dependency on stress level of the numerical mixtures is investigated. Results are compared with the documented behaviour of granular materials used for pavements and railways. Furthermore, the dependency of the permanent strains on the closeness of the applied load to the static failure stress is studied in accordance with the Technical Research Centre of Finland (VTT) shear-yielding material model (30). The correlation between fabric structure and performance is also analysed. This is covered by Publication III.

The three publications on which this part of the thesis is based are appended at the end of this thesis (see Appended papers, Publication I to III). Their complementary nature is illustrated in Figure 3.

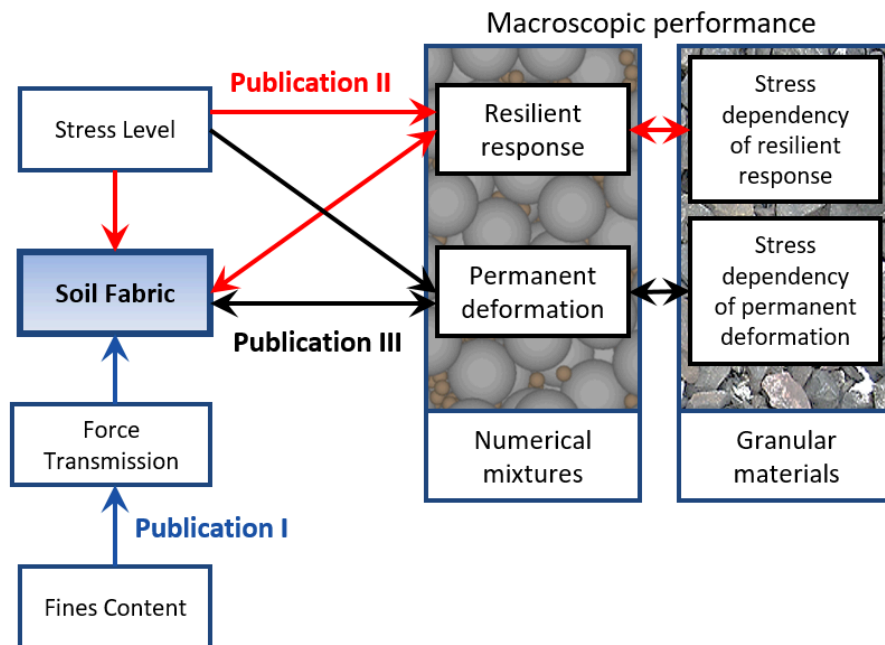


Figure 3. Schematic overview of relations between appended publications I, II and III. Single sided arrows $A \rightarrow B$ stand for studying the influence/effect of A on B. Double sided arrows $A \leftrightarrow B$ stand for investigating a possible correlation between A and B.

1.2.2 Limitations

It is a common approach to use DEM to directly replicate the observed response of real granular materials under laboratory testing conditions, where additional factors such as grain shape and angularity or particle degradation are present, e.g. (11,15). However, this investigation focuses on

idealized mixtures of elastic spheres and observing behavioural similarities with granular materials. As follows, elements constituting the numerical model, i.e. elastic spheres, should not be directly equated to single grains in UGM, but rather that the behaviour of the numerical assembly is partly corresponding to that of an assembly of real UGM. Models are always a simplified representation of reality or a part of it rather than reality itself; in other words, they idealise reality by making assumptions or simplifications about the world that are known to be false and hence should not be identified with reality². In fact, in order to facilitate or simplify the study and obtaining conclusions of a more general nature, the effect of particle shape and angularity has been purposely cancelled by considering spherical particles in this part of the study, even being this rather unrealistic for certain types of granular materials, especially crushed materials. However, models, when properly designed and implemented, can provide knowledge about the idealised world which may contribute to understand and make predictions about the real world. In this sense, it is the author's belief that the present work provides insight into the behaviour of idealized discrete materials and hence result in a better understanding of real granular materials.

1.3 Rockfill railway embankments

Compared with conventional railway ballasted tracks, it is commonly accepted that well-constructed slab-tracks generally result in significant lower settlements over the long term. This in turn results in lower maintenance costs for restoration of track geometry. However, once these settlements exceed a certain threshold, possibilities for routine un-expensive maintenance are much more limited for slab-tracks. For granular embankments, uncertainty on the development of settlements due to traffic loading exists within the embankment itself due to the inherent complexity of granular matter, as introduced in Section 1.1. It has also been mentioned that this complexity is mainly due to the discrete nature of the material, which becomes more relevant the larger the particle size in relation to the considered construction. This is especially the case for rockfill embankments, as these are constructed with blasted and/or crushed rock of relatively large particle size.

There is a lack of studies on full-scale measurements of settlements for rockfill railway embankments. Empirical studies concerning railway

² According to the Allegory of the Cave (72), it could be argued that models, as idealizations, belong to the world of *ideas* rather than to the physical world of change known to us only by our senses and hence part of the most fundamental kind of reality leading to true knowledge.

embankments are commonly based on scale model tests, e.g. (31,32). Full-scale studies on high rockfill embankments can actually be found for dams (33–35), where dam height has been long recognized as one of the most significant factors influencing settlements (35). Although dams present similarities with railway embankments, fundamental differences between these infrastructures exist, especially regarding loading mechanisms and even size scale. This greatly limits the applicability of studies on dams to the case of railway embankments under traffic loading. Nevertheless, it should be remembered that empirical studies alone would fail to provide a deeper insight into the micromechanics of granular matter behaviour and hence into the fundamentals governing its macroscopic response. On the other side of the spectrum, the same could in principle be said for continuum-based mechanistic methods as FEM, where fundamental micromechanical processes like particle rearrangement cannot be explicitly incorporated into the material model. With all the above considerations in mind, DEM presents a great potential to achieve a more profound understanding on the effect of different processes at particle level on the macroscopic mechanical response of rockfill embankments.

Among the main limitations of DEM is computational time, especially for large collections of particles under a high number of load cycles, i.e. the case for high rockfill embankments under traffic loading. Particle shape, i.e. level of geometrical complexity of the particles in the model to reproduce the shape and angularity of real particles, is also known to have a profound effect in computational time needs. In the case of common three-dimensional DEM models based on spherical particles and clumps of spheres, as is the case with PFC3D (36), it is obvious that an increasing number of spheres to represent a single particle results in increasing time demands. All the above can also be greatly aggravated by including particle degradation in the material model, especially if using the so-called bonded spheres technique as in Lu & McDowell (11,15). Albeit all the above presented challenges, studies do conclude on the need of clumps of spheres as opposed to individual spheres in order to capture the effect of interlocking on rearrangement and obtaining a more realistic response for railway ballast materials (15,37). Studies also show the importance of including degradation when modelling settlements of ballast materials (11,15,38). Therefore, DEM modelling of rockfill embankments under cyclic loading comes with great challenges.

Regarding particle shape and angularity, there are studies showing that simple clumps of spheres can result in realistic results (11,15,39) presenting a computationally efficient alternative to more complex irregular shapes trying to represent more realistic shapes for stone-based materials. In fact, the adequacy of complex irregular clumps has recently been explicitly questioned (39). Instead, simpler clumps are favoured, where simplifications are compensated, to some extent, by contact laws

where damage processes are included and where models are validated using different tests types and multiple measurements. Figure 4 visually illustrates the difference between complex irregular clumps and simpler regular clumps.

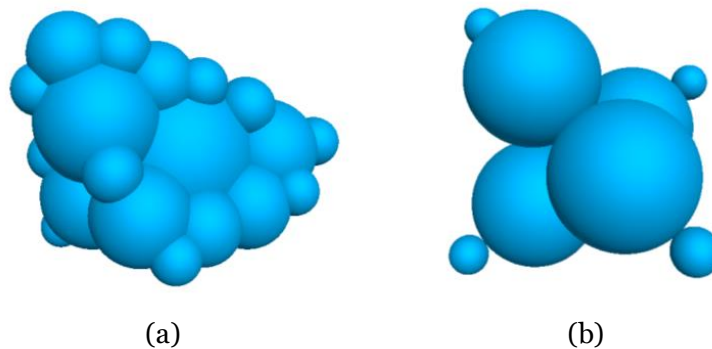


Figure 4. Example of (a) complex irregular clump and (b) simple regular clump for modelling particle shape.

Regarding degradation, breakage of ballast mainly takes place in the form of corner breakage, although particle splitting can also be observed (40,41). When using spheres (alternatively discs for 2D studies) and clumps of spheres, two families of explicit methods to account for breakage are generally used, referred here to as bonded clusters and breakable clumps. Particles can be modelled as clusters of bonded spheres where breakable bonds at contact points are used (36). This is a computational time consuming technique where intraparticle forces at the bonds need to be continually updated. This generally imposes the omission of particle splitting in order to cope with the increases in computational time needs (11,15). Furthermore, bonds are governed by numerous parameters without a clear physical interpretation that result in time consuming calibration processes. This renders the model rather vulnerable outside the conditions it is calibrated for. Particles can alternatively be modelled as “unbreakable” internally rigid clumps where breakage is represented by releasing selected spheres from the clump, effectively transforming these into “breakable” clumps. Internal contacts within clumps are ignored during calculations (36) resulting in considerable reductions in computational time needs compared to the use of clusters of bonded spheres. Furthermore, the triggering of breakage can be controlled by parameters such as the magnitude of the applied force and particle coordination number, i.e. number of contacts with neighbouring particles, e.g. (38,42,43). These are parameters with a much clear physical

interpretation and that are known to have a significant effect on particle breakage (44), having the potential to result in more robust models. However, all the above studies on breakable clumps are limited to 2D models.

There are three-dimensional modelling examples of railway ballast under triaxial conditions using DEM that besides include degradation (11,15). Triaxial tests allow to develop material models in a much reduced scale compared to modelling the whole ballast layer or rockfill embankment, which has a monumental impact on computational time needs. Triaxial testing for ballast materials has also been well documented, e.g. (40,41), allowing comparison with model results. However, the scale of the problem and boundary conditions in triaxial testing significantly defer to rockfill embankments. In particular, although nearly triaxial conditions may be assumed under the centre of the track, a free-slope condition exist for both the ballast layer and the embankment.

There are also three-dimensional studies where the ballast layer has been modelled using DEM (14,45,46), However, none of these studies included explicit modelling of particle degradation due to its additional computational cost when already dealing with a large assembly of particles. It should also be observed that these studies refer to the ballast layer, typically 30-40 cm thick measured from the underside of the sleeper. For embankments, i.e. rockfill material for the considered case laying between the frost protection layer and the foundation (see Figure 5), values up to 10 m are not uncommon.

All the above clearly highlights the vast difficulties associated with three-dimensional modelling of high rockfill embankments under cyclic loading, especially if particle degradation is to be explicitly included in the material model. As a matter of fact, despite all the advances in the use of DEM for modelling of granular matter over the last decade, no attempt to model a railway embankment has been undertaken before, to the best of the author's knowledge.

1.3.1 Aims and scope

In this second part of the thesis, high rockfill embankments are studied using DEM, with a certain emphasis on the slab-track configuration. In particular, the influence of embankment height and particle degradation on the macroscopic mechanical response to cyclic loading induced by traffic is investigated, namely settlements and resilient response. Figure 5 shows a simplified representation of a possible rockfill embankment for slab-track configuration.

Firstly, a DEM material model suitable for its implementation in large constructions of unbound stone-based materials is developed under triaxial conditions. Particles are based on simple regular breakable clumps.

Both corner breakage and particle splitting are included, where breakage processes are controlled by values of contact forces and coordination number. Model results are compared against experimental results for different triaxial test types and multiple measurements types on railway ballast, i.e. monotonic and cyclic testing using results for axial and volumetric deformations, as well as resilient response. All in all, it results in an efficient and robust model ideal for implementation in rockfill embankments. Results at particle level are also obtained and analysed in order to gain insight into the fundamentals of material behaviour. This is covered by Publication IV

Lastly, the developed breakable clumps are implemented in the actual modelling of rockfill railway embankments. Embankments with heights ranging between approximately 2 and 10 m are generated by successive dumping and compaction of layers of clumps on top of each other, mimicking the construction of real embankments. Cyclic loading of the embankments is undertaken for both breakable and unbreakable assemblies. The influence of embankment height and particle breakage on the mechanical response to cyclic loading, especially on settlements accumulation and resilient response, is studied. Results at particle level are used to provide explanations to the observed behaviour. This is covered by Publication V.

Figure 5 shows a schematic representation of a possible railway embankment cross-section for slab-track configuration. An emphasis has been placed on minimizing the embankment cross-section dimensions and advantage of different symmetry planes is taken in order to reduce the model size. The model focuses on the rockfill of the embankment, where only the coarsest fraction of the material is targeted to further reduce computational expenses.

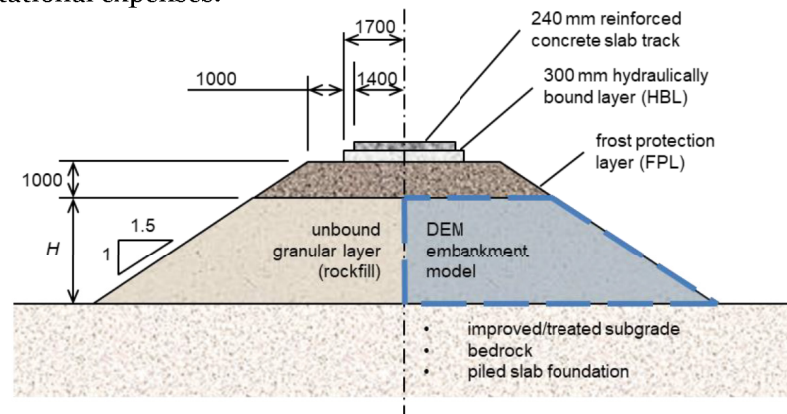


Figure 5. Schematic cross-section of rockfill embankment for slab-track configuration. All dimensions in mm.

1.3.2 Limitations

Numerous simplifications were needed to be able to realize the modelling of rockfill embankments, mostly intended to limit computational time. Among the most self-evident stands the fact of assimilating angular crushed rock particles to simple clumps of spheres. This is necessarily to be able to computationally handle large collections of particles. It has been argued that simple clumps of spheres can result in realistic results questioning the adequacy of more complex irregular shapes. Besides, clumps of spheres are unable to fully reproduce the angular shapes and rough textures present in crushed rock no matter how complex these clumps are. A substantial level of simplification would always be imperative.

Regarding particle breakage, the model is focussed on processes that can explicitly be implemented on clumps of spheres, namely corner breakage and particle splitting. Smaller scale processes like the grinding of small-scale asperities off the particle surface have not been considered. Previous studies did accommodate such processes by the use of interparticle bonds (11,15), which also partly accounted for the above mentioned lack of angularity inherent when using clumps of spheres. In these studies, the ballast layer was targeted, where acting deviatoric to confinement stress ratios are much higher than for the case of the deeper rockfill body. Permanent axial strain in granular materials can be correlated to the level of mobilised shear strength (5,30). Shear strength can in turn be correlated to particle angularity (47). For the high stress ratios in the ballast layer, the material is closer to utilising its full capacity, and therefore angularity plays a much more significant role than at the lower ratios present in the rockfill. Therefore the model is intended for the lower deviatoric to confinement stress ratios present in the rockfill and consequently the use of bonds to accommodate for additional angularity may be omitted.

No consideration to settlements originated outside the rockfill mass is given as only settlements within the rockfill are investigated. Besides, the implementation of slab-track in Sweden should be on a foundation free of settlements (48). Only settlements due to traffic loading are modelled. Possible long-term settlements due to creep within the rockfill mass are not specifically targeted to limit computational time needs.

The authors of the presented studies (Publications IV and V) are fully aware of the numerous simplifications and limitations embedded in the model. However, the model is deemed as a suitable tool to predict the order of magnitude of macroscopic responses and level of significance of influencing factors. This is especially advantageous when a lack of full-scale measurements exists. Moreover, if validated against full-scale results,

the model can be used to provide explanations at particle level which empirical testing alone will fail to provide.

1.4 Outline of the thesis

This thesis is based on the five appended publications with the addition of setting a common context for the overall research. It starts with a general background on the importance and complexity of granular materials for infrastructures and how DEM can help towards a better understanding of the fundamentals of granular matter. It continues by setting the scope, aims and limitations of the research together with the rationale of the adopted approach for the two considered questions, i.e. (i) soil fabric and performance and (ii) high rockfill embankments. The thesis also outlines the proposed soil fabric classification system and the developed material model for rockfill embankments. Numerical procedures and main results and conclusions for both topics are summarized as well, including a few additional complementary results, background information and discussions not included in the appended publications. It finishes with some concluding remarks highlighting the main scientific contributions of the work and suggestions for further research.

Publication I: Force Transmission and Soil Fabric of Binary Granular Mixtures

The effect of fines content on force transmission and soil fabric development of binary mixtures of elastic spheres under triaxial compression is studied using DEM. Results at particle level are used to define load-bearing soil fabrics where the relative contributions to resist the applied deviator stress of the different contact-type networks are explicitly quantified.

Publication II: Resilient Properties of Binary Granular Mixtures

The effect of stress level on the resilient modulus of binary mixtures of elastic spheres under triaxial loading is investigated using DEM. Results are statistically compared with existing relations characterizing the stress dependency of the modulus for real granular materials. Furthermore, the stress dependency of the soil fabric classification system proposed in Publication I is studied and its correlation with performance is statistically assessed.

Publication III: A Numerical Study on the Permanent Deformation of Gap-Graded Granular Mixtures

The effect of stress level and soil fabric structure on the permanent strain response of binary mixtures of elastic spheres under triaxial loading is investigated using DEM. Numerical results are compared with the

laboratory determined behaviour of granular materials. Additionally, mixtures are loaded to static failure to study the dependency of the permanent strains on the closeness of the applied stress to failure stress, in accordance with existing empirical models.

Publication IV: A Discrete Element Material Model Including Particle Degradation Suitable for Rockfill Embankments.

Compared with previous modelling efforts of railway ballast under triaxial conditions using DEM, a more computationally efficient and robust model suited for implementation in high rockfill embankments is presented. The model considers both corner breakage and particle splitting, something unique when modelling three-dimensional assemblies of particles. Results under different triaxial loading protocols are compared to experimental results for multiple measurements types. Results at particle level are used to gain insight into the fundamentals of material behaviour.

Publication V: Discrete Element Modelling of Rockfill Railway Embankments.

The material model developed in Publication IV is implemented in the actual modelling of rockfill embankments. Embankments with heights ranging between 2 and 10 m are generated by mimicking the construction of real embankments. Cyclic loading of the embankments representing railway traffic, for both breakable and unbreakable assemblies, is undertaken. The influence of embankment height and particle breakage on the mechanical response to cyclic loading, especially on settlements accumulation and resilient response, is studied. Results at particle level are used to provide explanations to the observed behaviour.

2. Soil fabric and performance of binary mixtures

In this section, the soil fabric and its effect on performance are investigated, with a certain emphasis on base and sub-base unbound layers for flexible pavements as used in Sweden. This part corresponds with publications I-III.

2.1 Soil fabric classification system

Based on previous studies using DEM by Thornton and Zhang (49), the cumulative contribution to the different components of the overall stress tensor of the individual interparticle contact forces of an ensemble of spheres can be evaluated with:

$$\sigma_{ij} = \frac{1}{V} \sum_{N_c} [(R_1 + R_2) f_n n_i n_j + (R_1 + R_2) f_t n_i t_j] \quad (2)$$

where the summation extends to the total number of interparticle contacts N_c within the specimen volume V , being R_1 and R_2 the radii of the contacting spheres, f_n and f_t the magnitudes of the normal and tangential components of the contact force, respectively, and n_i and t_i the unit vector components of the normal and tangential contact forces, respectively.

For the case of principal components of the stress tensor, equation (2) can be simplified to:

$$\sigma_{ii} = \frac{1}{V} \sum_{N_c} (R_1 + R_2) n_i (f_{n,i} + f_{t,i}) \quad (3)$$

where $f_{n,i}$ and $f_{t,i}$ are component i of the normal and tangential forces, respectively. In turn, for the case of triaxial loading, this allows the corresponding contact forces' cumulative contribution to the deviator stress to be obtained as:

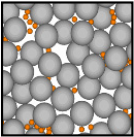
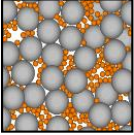
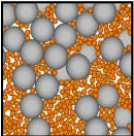
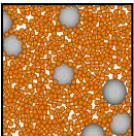
$$\sigma_d = \sigma_{11} - \frac{\sigma_{22} + \sigma_{33}}{2} \quad (4)$$

For gap-graded mixtures, Minh et al. (50) showed that N_c can be further decomposed into three types of interparticle contacts, namely the coarse-to-coarse $c-c$, coarse-to-fine $c-f$ and fine-to-fine $f-f$ networks. This allows to determine the contribution of each individual network in resisting the applied deviator:

$$\sigma_d = \sigma_d^{c-c} + \sigma_d^{c-f} + \sigma_d^{f-f} \quad (5)$$

The first and last components, σ_d^{c-c} and σ_d^{f-f} , represent the contribution of the coarse and fine grain skeletons, respectively, whereas σ_d^{c-f} measures the contribution of their interaction. Based on the relative contribution of each network, a soil fabric classification system is proposed in Publication I similar to existing classification systems (28,29). Its main novelty is that soil fabric cases are explicitly characterized in terms of contact force transmission at particulate level rather than inferred from the observed macroscopic response and macroscopic volumetric indexes. Table 1 summarizes the proposed system. A more thorough description of the soil fabric cases can be found in the Introduction of Publication II.

Table 1: Soil fabric classification system for the study of load-bearing mechanisms of gap-graded granular mixtures after de Frias et al. (Publication I)

Fabric case	Fabric characterization	Description	Schematic illustration
(A) Underfilled	$\sigma_d^{c-c} > \sigma_d^{c-f}$ $> \sigma_d^{f-f}$	Coarse grain supported structure with small amount of fines <i>underfilling</i> the voids between coarse particles	
(A-1) Underfilled-instable			
(B) Interactive-underfilled	$\sigma_d^{c-f} > \sigma_d^{c-c}$ $> \sigma_d^{f-f}$	Strong interaction between fractions with fines near-optimally filling the voids between coarse particles	
(C) Interactive-overfilled	$\sigma_d^{c-f} > \sigma_d^{f-f}$ $> \sigma_d^{c-c}$	Strong interaction between fractions with fines slightly <i>overflowing</i> the voids between coarse particles	
(D) Overfilled	$\sigma_d^{f-f} > \sigma_d^{c-f}$ $> \sigma_d^{c-c}$	Small amount of coarse particles floating in a matrix of fine particles	

In particular, the instable fabric (A-1) represents a special underfilled subcase where, owing to a relatively low content of fines, single fine grains become trapped between coarse particles aligned along the main loading direction, creating a potential for instability. According to previous suggested explanations, for very low FC , the number of trapped particles may be not enough to produce a significant effect whereas for higher FC , there are too many fine particles preventing this phenomenon (50). Essentially, instable fabrics can be identified based on the minimum cumulative contributions of the different contact-type networks to the deviator stress or on the probability density distribution PDD of normal contact forces (50). However, comparison of both methods in Publication II proved the former difficult to implement for low deviator to confinement stress ratios, suggesting the latter as more reliable. The importance of identifying this fabric stems from an expected reduced performance as consequence of its instable load-bearing structure.

2.2 Particle size ratio

Computational time is a major concern when performing simulations with DEM. This greatly increases with the number of particles. Therefore, in order to partly overcome this, the particle size ratio PSR for the binary specimens, i.e. the ratio between the coarse and fine grain sizes D_c/D_f , is minimized based on crystallography as follows.

The size of the largest sphere that can occupy the smallest void in a closed-packed structure, i.e. the densest possible packing of equal sized spheres of diameter D , is given by $0.225D$ (51). This PSR, i.e. $D_c/D_f = 4.44$, may be regarded as a theoretical limit below which fine particles start becoming relatively too big to be able to occupy the voids within a dense packing of coarser particles without greatly disrupting its contact network, i.e. becoming a separator of coarse grain contacts, and turning both fractions into effectively the same. In fact, this value has been suggested in previous research as a limit to define interacting fractions for pavement design (26,27). The use of any PSR value higher than 4.44 causes an increase in number of fine particles and an associated increase in computational time for any given FC . Figure 6 illustrates the relative sizes of the particles fitting into the smallest and largest possible voids within a closed-packed structure, namely tetrahedral and octahedral voids respectively.

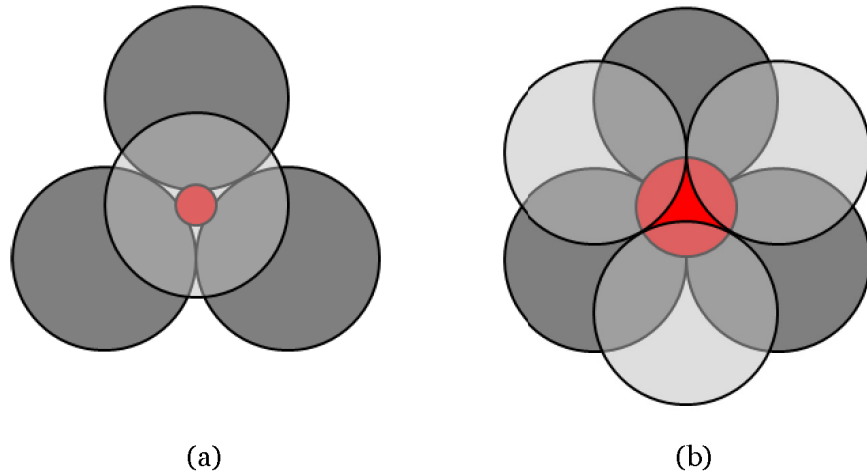


Figure 6. Top view of closed-packed structures showing relative sizes of particles (D) and spheres fitting into (a) tetrahedral void ($0.225D$) and (b) octahedral void ($0.414D$). Particles in grey (bottom layer dark grey and top layer light grey) and spheres fitting voids in red.

2.3 Numerical procedures

A brief description of the procedures for specimen generation and loading implemented with the DEM software PFC3D v4.0 (36) is presented below. More detailed information can be found in Publications I-III

Bidisperse compacted mixtures of elastic spheres, with fines contents ranging from 0 to 100% in steps of approximately 10% and low isotropic stress, were generated within cylindrical containers with a height to diameter aspect ratio of 2.0. Specimen dimensions were chosen as a compromise between computational time and size dependency of the system response. A linear elastic contact law with Coulomb friction was implemented (36) where the particle normal stiffness k_n was assigned as a function of its radius R and a constant contact elastic modulus E_c :

$$k_n = 4 \cdot E_c \cdot R \quad (6)$$

The use of this scaling relation makes the specimen's behaviour unaffected by absolute values of particle sizes. Two specimens with proportional PSDs, i.e. identical PSRs and FC for the case of binary mixtures, should behave almost identically independently of maximum particle size (possible small differences are attributed to the stochastic nature of the random placement of spheres during the generation

procedure). It must be stated that this non dependence on grading scale is not necessarily the case for granular materials, e.g. (52).

The sample generation procedure was based on particle inflation in a similar fashion as described in Itasca (36). Basically, the material vessel is first filled with a dense packing of partially overlapping frictionless spheres with random placement. This is followed by relaxation of the assembly and installation of a low isotropic mean normal stress p_0^t by uniformly reducing the radii of all particles in iterative manner following the procedure described in Itasca (36). Specimens are finalised by assigning the selected friction coefficient μ to all particles. The main input micromechanical properties are summarized in Table 2, where properties are partly based on representative values for a Swedish crushed granite pavement subbase material as reported by Ekblad & Isacsson (53). More details on specimen generation can be found in Publication II.

Table 2: Micromechanical input parameters

Property	Value
Coarse particles diameter D_c	7.03 mm
Fine particles diameter D_f	1.58 mm
Contact elastic modulus E_c	400 MPa
Normal to shear particle stiffness ratio k_n/k_s	1.0
Wall normal stiffness $k_{n,wall}$	$1.0\bar{k}_n$
Particle friction coefficient μ	0.5
Wall friction coefficient μ_{wall}	0
Particle density ρ	2600 kg/m ³
Initial target stress p_0^t	2 kPa

After generation, all specimens were subjected to triaxial monotonic loading and unloading for the stress levels in Table 3. The corresponding stress paths are shown in Figure 7. A few selected specimens were cyclically loaded for a total of 100 cycles for stress level 1 (cf. to Table 3). This is done in order to investigate the possibility of using the secant stiffness during first unloading as an estimate of the long term resilient modulus after

several loading cycles for the considered conditions, i.e. assemblies of spherical particles far from shear-yielding failure, as this would result in significant savings in computational time. Additionally, all specimens were loaded to failure at a confinement of 100 kPa to analyse the dependency of the permanent strains on the closeness of the applied load to the static failure stress in accordance with the VTT model (30).

Table 3: Stress levels for monotonic triaxial tests

Test id.	σ_c [kPa]	σ_d [kPa]	p [kPa]	σ_d/σ_c	p/σ_d
1*	100	100	133.3	1.0	1.33
2	100	50	116.7	0.5	2.33
3	50	50	66.7	1.0	1.33
4	50	25	58.3	0.5	2.33
5	125	25	133.3	0.2	5.33
6	62.5	12.5	66.7	0.2	5.33
Failure**	100	$\sigma_{d,u}$	-	-	-

p : mean normal stress ($\sigma_c + \sigma_d/3$)

* selected specimens cyclically loaded for a total of 100 load cycles

** specimens loaded to total axial strain ε_a of 5 mm/m

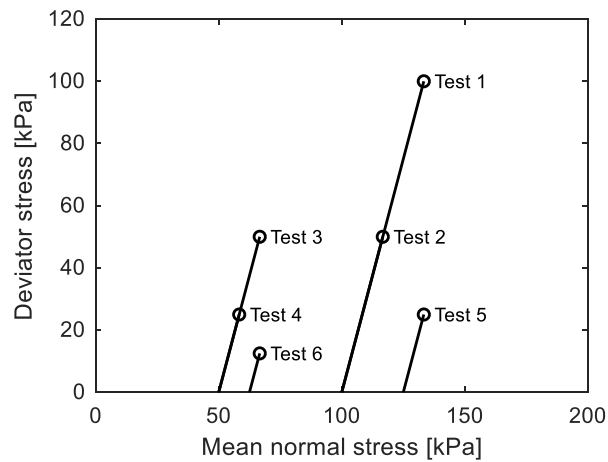


Figure 7. Stress paths for monotonic triaxial tests (cf. to Table 3).

Confining stresses were applied using the numerical servo-control mechanism described by Itasca (36). Specimens were then loaded by the top and bottom walls acting as loading platens, where these are progressively accelerated until achieving an axial strain rate $\dot{\epsilon}_a$ of 0.01 s^{-1} . Subsequently, strain-controlled loading continues at constant strain rate until the selected deviator stress was applied (for tests to failure, the loading continued until a specified value of axial strain was obtained). Contact forces were recorded at the peak of the loading process for subsequent analysis. Finally, specimens were unloaded by reversing the direction of the loading platens in similar conditions to the loading phase until the deviator became zero. The procedure was repeated for a total of 100 cycles for selected specimens under stress level 1 as indicated above. More details can be found in Publications I to III.

2.4 Results and discussions

The main results regarding specimen generation, soil fabric identification and macroscopic performance are presented below, together with discussions on the main conclusions and the effect of soil fabric on performance.

2.4.1 Specimens

Table 4 summarizes the main properties of the generated specimens, where the total number of particles ranges between 35307 and 69448. Figure 8 shows the effect of the fines content on the porosity of the generated specimens. The mixtures developed a smooth transitional zone of lower porosities around $FC \sim 30\%$, indicative of maximum packing potential in agreement with previous experimental and numerical findings (28,50). It must also be observed that the porosities for the monodisperse cases, 0.369 and 0.368 for FC00 and FC100, respectively, are very close to the minimum porosity that can be achieved by a random packing of hard spheres in three dimensions, i.e. 0.366 (54). This indicates that the generation procedure results in a densely packed state. Figure 9 shows examples of generated specimens.

Table 4: Specimens dimensions, number of particles, particle sizes and fine contents for generated cylindrical specimens (height to diameter aspect ratio $H_{\text{spc}}/D_{\text{spc}} = 2.0$); specimens denoted by nominal fines content

Specimen	H_{spc} [mm]	$N_{\text{p,c}}$ [-]	$N_{\text{p,f}}$ [-]	D_c [mm]	D_f [mm]	FC [%]
FC00	400	46053	-	6.90	-	0
FC10	200	5673	48362	6.88	1.55	8.8
FC20	160	2786	53433	6.90	1.55	17.9
FC30	120	1090	34217	6.88	1.55	26.3
FC40	120	917	46435	6.90	1.55	36.5
FC50	120	761	58002	6.89	1.55	46.4
FC60	120	595	68853	6.91	1.55	56.8
FC70	100	259	45631	6.91	1.55	66.6
FC80	100	170	51379	6.92	1.56	77.4
FC90	100	83	57804	6.92	1.55	88.7
FC100	100	-	63122	-	1.55	100

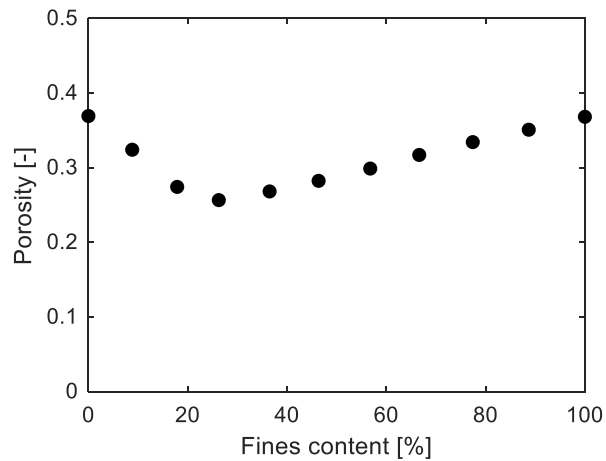


Figure 8: Effect of fines content on porosity of generated specimens

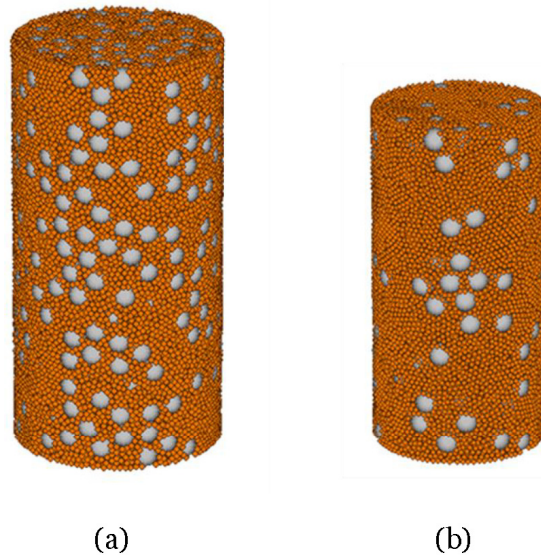


Figure 9: Examples of generated specimens for nominal fines content of (a) 40% (FC40) and (b) 70% (FC70). See Table 4 for further details on specimen dimensions and properties

2.4.2 Soil fabric

The formulation in Section 2.1, i.e. Equations (2)-(4), allows for the overall cumulative contribution to the deviator stress of the interparticle contact forces to be obtained. Additionally, the contribution of each individual contact-type network, i.e. the $c-c$, $c-f$ and $f-f$ networks, can be obtained.

Relative cumulative contributions for all specimens under stress level 1 (cf. to Table 3) are summarized in Figure 10, where soil fabrics and their limits according to Table 1 are included. The $c-c$ contribution is dominant for FC below 20%. This is followed by a sharp drop together with a steep increase in $c-f$ contribution, the latter becoming dominant with a near-flat contribution for intermediate FC . For FC over 55%, $f-f$ contacts become dominant. Similar conclusions can be obtained for all other stress levels in Table 3, where the cumulative contributions are nearly identical for any given deviatoric to confinement ratio. Differences between stress ratios are mostly noticeable in slight changes in the FC defining the limit between the interactive fabrics B and C, varying between 33 and 39% for stress ratios of 0.2 and 1.0, respectively (see Publication II).

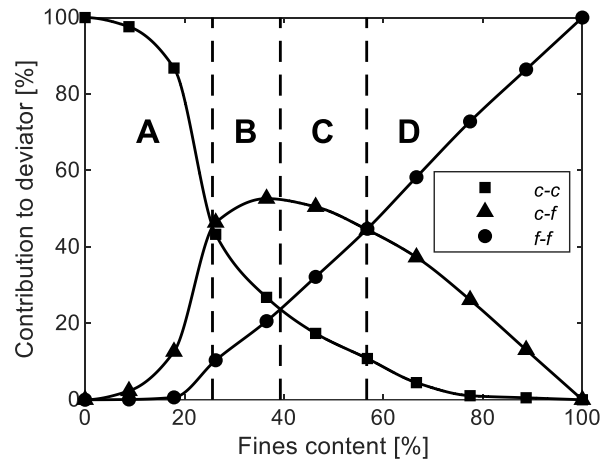


Figure 10: Contact-type networks' contributions to resist the applied deviator stress for stress level 1 including soil fabric limits (vertical dashed lines)

Underfilled-instable soil fabrics can be detected based on a distinct probability density distribution PDD function of the normal contact forces under loading when compared with other fabric cases (50). Figure 11 shows the PDD of the interparticle normal contact forces for stress level 1, where normal forces f_n are normalised by the average normal force for the system $\langle f_n \rangle$, for a normalised interval of 0.1. According to the above, FC20 can clearly be identified as instable, whereas FC10 shows some signs of instability, suggesting a situation where the number of fine grains trapped between coarse particles aligned along the deviatoric direction is starting to be enough to produce a significant adverse effect (see Section 2.4.5). Publication II also studied an existing alternative method for instability detection based on the minimum cumulative contribution values of the contact-networks (50). The latter was shown to be difficult to implement at low deviator to confinement stress ratios, where a clear distinction between the roles of weak and strong contacts does no longer apply. On the other hand, the method based on PDD proved to be more robust to changes in stress level.

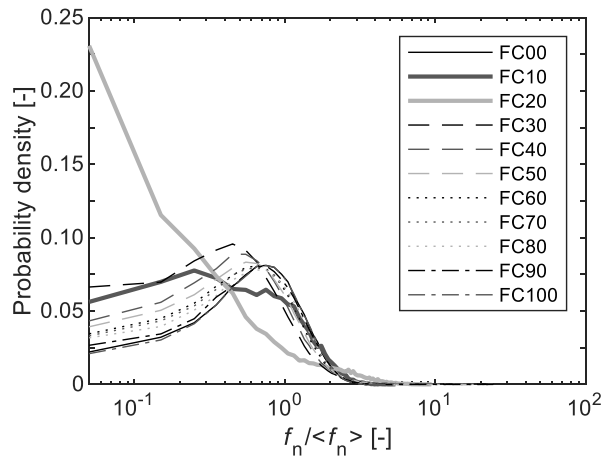


Figure 11: Probability density distribution of normalised normal contact forces for stress level 1

Table 5 provides additional information on normal contact forces not included in the appended Publications. It shows a wide range of average and maximum normal forces for the studied mixtures, highlighting the convenience of plotting PDD based on normalised forces to allow for curve comparison and detection of instable fabrics.

Table 5: Number of contacts, maximum and average normal contact forces for stress level 1

Specimen	N_c [-]	$\max f_n$ [N]	$\langle f_n \rangle$ [N]	$\max f_n / \langle f_n \rangle$
FC00	128163	23.27	5.83	3.99
FC10	17704	29.39	5.53	5.31
FC20	21152	24.84	2.64	9.39
FC30	76665	10.30	0.49	21.14
FC40	119985	7.60	0.38	20.23
FC50	154854	8.15	0.34	24.04
FC60	187034	7.46	0.32	23.31
FC70	124146	7.36	0.31	23.48
FC80	140850	5.23	0.31	17.00
FC90	160057	7.22	0.30	24.29
FC100	177037	1.41	0.29	4.85

Publication I compared the limit between interactive-underfilled and interactive-overfilled fabrics (B and C) for stress level 1 based on contact forces with limits from different macroscopic volumetric indexes according to existing classification systems, i.e. Vallejo (28) and Thevanayagam et al. (29). Results for stress level 1 showed a poor correlation for the limit based on the theoretical minimum porosity (28) ($FC \sim 39\%$ compared to 27% based on minimum porosity). However, a higher degree of correlation was shown for the limit based on the threshold fines content FC_{th} (29), close to 37% . Although stress level is not accounted for in FC_{th} and the underfilled-overfilled fabric limit is slightly sensitive to stress level variations (33 to 39% FC as shown above), FC_{th} still remains as a good predictor for the whole range of tested stress levels.

2.4.3 Resilient modulus

Stress level is the most significant structural factor influencing the resilient modulus (4). Table 6 shows some statistical models commonly used to describe the stress dependency of the modulus. In order to study the stress dependency of M_r for the numerical mixtures, all specimens were subjected to triaxial loading according to the stress levels in Table 3 and results statistically compared with the models in Table 6 considering the following (see below).

For granular materials, the resilient response is generally determined as the secant modulus during unloading after a certain number of load applications, ranging from hundreds to thousands. This initial phase, commonly referred to as sample conditioning, is needed in order for the sample to reach a stable resilient behaviour. Owing to the spherical shape of the numerical particles in this study, the secant stiffness during first unloading, i.e. monotonic loading, is proposed as an estimate of the long term modulus after several loading cycles to reduce computational time. Figure 12 summarizes the results. On a later stage, few selected specimens were subjected to 100 load cycles under stress level 1 showing monotonic values to be rather accurate estimators of the long term modulus for well-compacted assemblies of elastic spheres. For the cyclic tests, conditioning took almost entirely place during the first loading cycle (see as example Figure 13 where an almost purely resilient behaviour seems to be reached already during the first unloading). Therefore the modulus during first unloading was indeed an accurate and computational-time efficient estimator of the long term modulus (e.g. for specimen FC40, testing 100 load cycles took approximately 12 days compared with roughly 4 hours for monotonic loading). The spherical shape of the particles together with the closely-packed initial state of the system are speculated to be the main

reasons for the observed rapid conditioning. Additionally, the absence of particle degradation is expected to have further contributed to the above.

Table 6: Commonly used models describing the stress dependency of the resilient modulus for triaxial loading conditions

Model	Expression	Eq. No.
Dunlap (55)	$M_r = k_1 \sigma_c^{k_2}$	(7)
Pezo (56)	$M_r = k_1 \sigma_c^{k_2} \sigma_d^{k_3}$	(8)
Seed et al. (3)	$M_r = k_1 p^{k_2}$	(9)
Uzan (57)	$M_r = k_1 p^{k_2} \sigma_d^{k_3}$	(10)

σ_c : confinement stress
 σ_d : deviator stress
 p : mean normal stress ($\sigma_c + \sigma_d/3$)
 k_1, k_2, k_3 : regression constants unique to each function and material

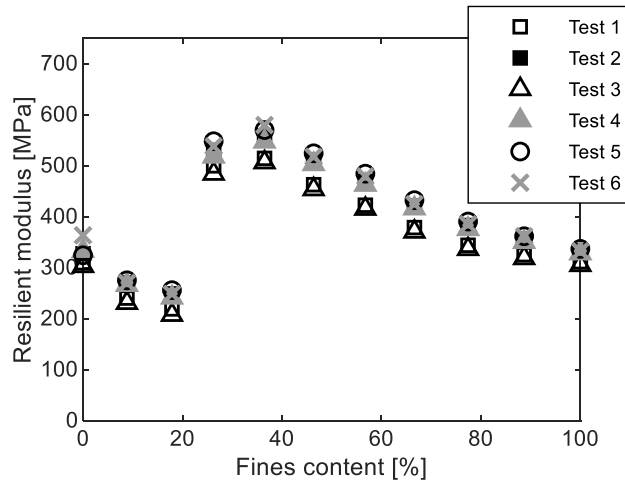


Figure 12: Effect of stress level and fines content on the resilient modulus after monotonic triaxial loading (cf. to Table 3 for stress levels)

For each fines content value, results after monotonic loading for the six tested stress levels in Figure 12 were fitted to the models in Table 6 by means of minimizing the sum of square errors. Statistical analysis of the results showed a significantly better agreement between the numerical

specimens' behaviour and that described by the Pezo and Uzan models compared to the unidimensional models. The average coefficient of determination R^2 for all specimens was 82% for Pezo and 80% for Uzan. Furthermore, the Pezo model could be simplified to $k_3 = -k_2$, i.e. $M_r = k_1(\sigma_d/\sigma_c)^{k_2}$, indicating a marked dependence of the modulus with the deviator to confinement stress ratio for the numerical specimens. The fines content also showed a significant statistical effect on the modulus (see Section 2.4.5). Details of the statistical analyses can be found in Publication II.

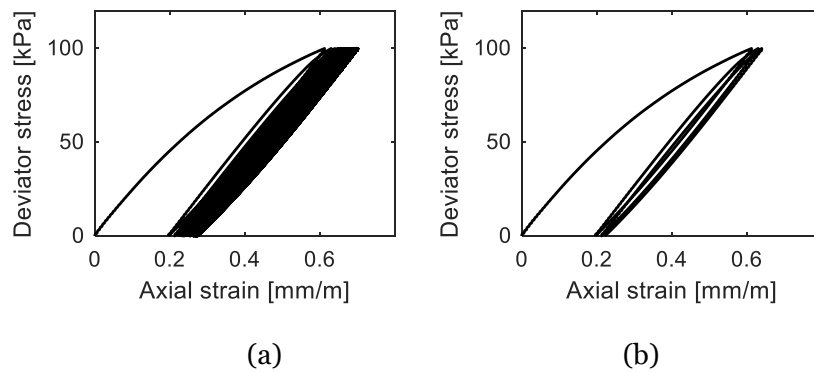


Figure 13: Cyclic triaxial loading stress-strain response for specimen with nominal fines content of 10% (FC10) under test series 1 stress level for (a) 100 load cycles and (b) detail for first 3 load cycles

2.4.4 Permanent deformation

The effect of stress level on the permanent deformation of the numerical mixtures is presented in this section and results are compared to the behaviour of granular materials used for pavements and railways. Figure 14 summarizes the permanent deformations after monotonic triaxial loading according to the stress levels in Table 3, whose stress paths in the $p - q$ plane are shown in Figure 7. For any given fines content, permanent strains grow with the ratio of applied deviatoric to confinement stress, a pattern characteristic of pavement UGM and railway ballast (58–60). Additionally, for any given stress ratio, an increase of the stress path length, defined as the length between the minimum and maximum deviators in the $p - q$ space (see Figure 7), generally results in higher permanent strains. This is common to ballast materials (60) and granular materials for pavement structures (61,62), differences being more dramatic for higher stress ratios. The influence of stress on permanent

strains is illustrated in Figure 15, where the multidimensional effect of stress ratio and stress path length is shown for specimen FC30 (similar behaviour can be observed for other specimens).

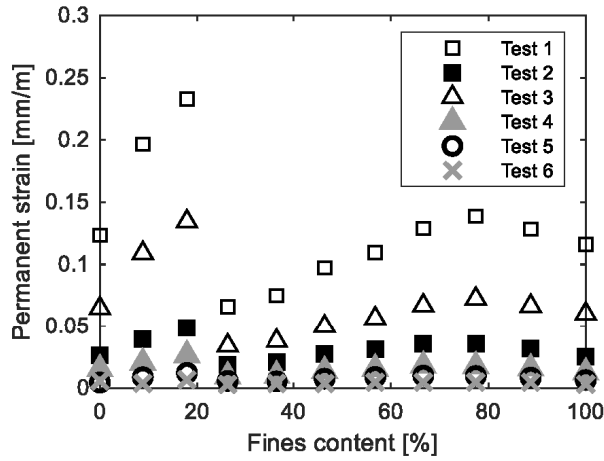


Figure 14: Effect of stress level and fines content on the permanent deformation after monotonic triaxial loading

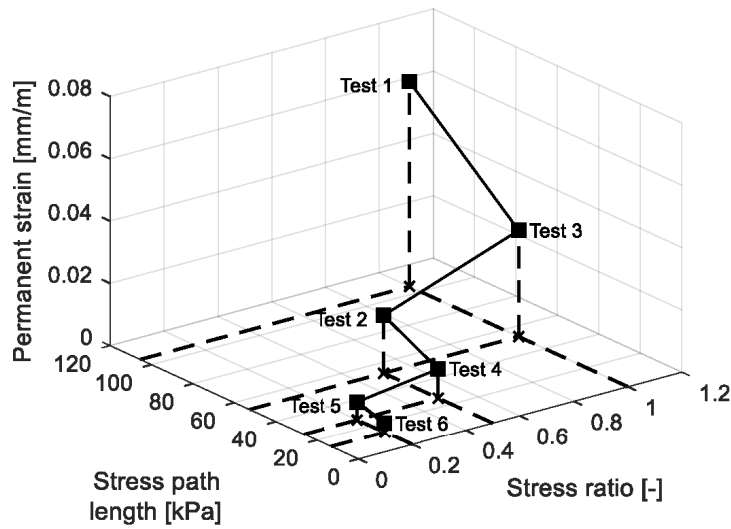


Figure 15: Effect of deviator to confinement stress ratio and stress path length on permanent deformation after monotonic triaxial loading for FC30

In order to further compare the stress dependency of the permanent deformation of numerical mixtures with that of granular materials, the dependency of ε_p on the closeness of the applied load σ_d to the static failure stress $\sigma_{d,u}$ is studied in accordance with the VTT model (30):

$$\varepsilon_p = B \left(\frac{R_u}{A - R_u} \right) \quad (11)$$

where R_u is the failure ratio ($\sigma_d/\sigma_{d,u}$), A the maximum possible value of R_u (theoretically 1.0) and B a stress dependent material parameter. The model is considered valid for both monotonic and cyclic loading, except for incremental collapse conditions (30).

To determine failure stress, all specimens were loaded until development of a total axial strain of 5 mm/m under $\sigma_c = 100$ kPa. This allowed to determine R_u for all specimens under stress levels 1 and 2. The effect of R_u on the permanent deformation is illustrated in Figure 16, where results are fitted to the VTT-model according to equation (11) with $A = 1.0$ and $B = 0.086$ mm/m obtained by minimizing the sum of square errors. A fairly strong correlation between numerical results and the VTT-model is obtained ($R^2 = 0.80$) showing again that numerical mixtures were able to reproduce some of the most significant features of granular materials regarding permanent strain response to stress level.

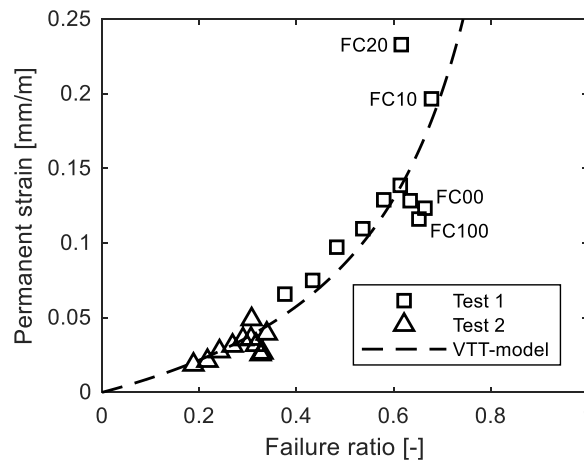


Figure 16: Effect of failure ratio on permanent deformation ($\sigma_c = 100$ kPa)

2.4.5 Soil fabric and performance

The two previous sections have established a certain degree of resemblance between the stress dependency of resilient modulus and permanent deformation of the numerical mixtures and UGM for highway and railway applications. This section studies the possible correlation between macroscopic performance and the soil fabric (Section 2.4.2). It must be observed that the soil fabric classification system presented in Publication I was based exclusively on micromechanical considerations regarding force transmission at particulate level, and without any regards to macroscopic performance aspects.

Statistical analysis of the effect of fabric structure on the resilient modulus after one loading cycle showed that indeed the soil fabric was a significant source of variation. Further analysis concluded that three significantly differentiated levels of resilient response could be established:

- Significantly stiffer response is observed for interactive fabrics (B & C) with no significant difference between them
- Significantly softer response is observed for instable fabrics (A-1)
- Base level of performance, i.e. an intermediate response between the above fabrics, is observed for underfilled (A) and overfilled (D) fabrics, being the former slightly softer than the latter.

In particular, within the instable fabric cases, specimen FC20 showed a lower modulus than FC10 (see Figure 12). This further supports the explanations provided in Section 2.4.2 according to which FC20 showed a higher degree of instability than FC10 based on the PDD of normal contact forces.

Permanent strain results for monotonic loading in Figure 14 show that, in general:

- Interactive fabrics show lowest permanent strain values
- Instable fabrics show the highest permanent strain values
- A base level of performance is observed for underfilled and overfilled fabrics
- Observed differences are larger at higher deviator to confinement stress ratios and stress path lengths.

Additionally, within the instable fabric cases, specimen FC20 showed higher deformations than FC10 in agreement with the explanations provided suggesting a higher degree of instability for FC20.

Table 7 summarizes the effect of soil fabric on both of the studied aspects of performance. It can be concluded that a gradation resulting in a fabric structure where the structural interaction between the coarse and fine fractions is maximized, i.e. interactive fabrics, ultimately translates into performance improvements.

Table 7: Effect of soil fabric on macroscopic performance

Fabric case (Publication I)	Resilient response (Publication II)	Permanent deformation response (Publication III)
Underfilled (A)	base level; slightly softer response than overfilled fabrics	base level
Underfilled- instable (A-1)	significantly softer response	highest deformation
Interactive (B & C)	significantly stiffer response	lowest deformation
Overfilled (D)	base level; slightly stiffer response than underfilled fabrics	base level

3. High rockfill railway embankments

In this section, high rockfill railway embankments, with an emphasis on slab-track configurations, are studied using DEM. The influence of embankment height and different processes at particle level, like particle breakage, on the mechanical response to traffic induced loading are investigated. This part corresponds with publications IV and V.

3.1 Particle degradation

In this thesis, only mechanical degradation or disintegration as result of mechanical forces transmitted via inter-particle contacts is considered. Other types of particle degradation, such as weathering, fall outside the scope of this thesis.

In this chapter, a summary of the main types of mechanical degradation is presented together with a brief discussion on some of the main factors influencing their relative importance and effect on the material macroscopic behaviour. The algorithm for the implementation of the selected degradation processes in DEM is also summarised. This is the algorithm that is presented and developed under triaxial conditions in Publication IV and later implemented for embankment modelling in Publication V. A more detailed description of the algorithm itself can be found in Publication IV.

3.1.1 Main processes, factors and significance

The mechanical degradation or disintegration of granular materials can be divided into three main processes regarding the size ratio of the broken product to the original particle (44):

1. the grinding of small-scale asperities off the particle surface
2. the breakage of corners or angular projections
3. the breakage or splitting of particles into approximately equal parts

The above processes are obviously greatly influenced by the magnitude of the applied force. The first process is generally the case for low values of contact forces resulting in attrition whereas breakage occurs at higher contact forces. The relative importance of these is also dependent on particle shape. For example, rounded non-crushed particles will mainly experience type 3 breakage same as for flaky or elongated particles resulting from crushed aggregates. Equidimensional highly angular crushed material, as the one generally used for railway ballast, will

experience mostly degradation in the form of particle abrasion and corner breakage, e.g. (40,41).

Other than particle shape, both particle size and coordination number, which relates to the loading configuration, are known to play a significant role (63). Large particles have a lower survival probability as their probability of containing more and larger internal flaws becomes higher when compared with smaller particles. However, particle size may be of a lesser significance compared to angularity (64). Particle fracture is associated with induced tensile stresses in the particle, which will reduce with an increase in the coordination number. This is due to the compressive stresses caused by additional contacts. The effect of confining pressure, which in turn influences the coordination number, has also been highlighted (40,41), partly governing the relative importance of the different degradation processes in railway ballast materials.

Additionally to the numerous involved factors, the effect of degradation is not straightforward and is greatly influenced by the relative importance of the three aforementioned processes. Although degradation may initially lead to a reduction in particle interlock and inter-particle surface friction, densification may also occur resulting in further points of contact where additional shear resistance may be mobilized. Furthermore, abrasion and attrition of granular surfaces result in powder generation which contributes to fouling and possible lubrication of interparticle contacts. In the presence of water, slurry may be formed greatly exacerbating the lubrication.

3.1.2 DEM implementation

An algorithm has been developed and written for PFC3D v4.0 (36) in order to incorporate degradation in Publication IV. The algorithm focusses exclusively on those processes that can easily be explicitly included when representing particles by simple clumps of spheres, i.e. corner breakage and particle splitting.

The algorithm is intended for clumps. A clump is a collection of slaved spheres constituting a single particle or entity in the model that is rigid internally but with a deformable external boundary. Internal contacts are ignored during calculation as clumps are rigid internally. This means a substantial reduction in computational needs, at the expense of being the clump unbreakable by definition. Clumps of spheres allow for explicitly including interlocking derived from non-spherical shape in the simulations. For the present case, clumps are to be formed by a collection of four spheres constituting what may be called the main body of the particle and to which four smaller size spheres are added on its contour, constituting what may be called the asperities, altogether forming a rigid clump, see Figure 17. In the present work (Publications IV and V),

asperities have a radius of 0.35 the radius of the balls comprising the clump body similarly to (11,15).

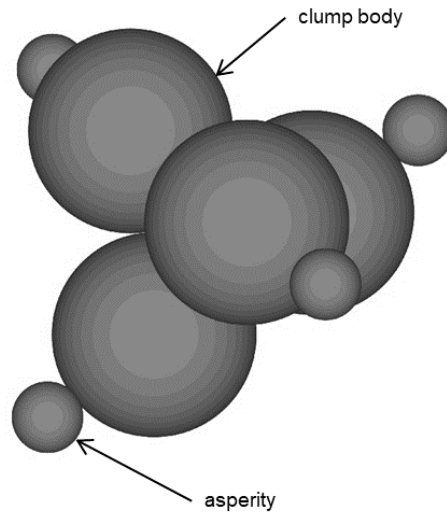


Figure 17. Regular tetrahedral clump with four asperities

The algorithm starts assigning fracture normal contact force $f_{n,f}$ values to all balls together with a minimum coordination number $C_{n,min}$ value to all clumps above which these are no longer liable to experience splitting. Values of $f_{n,f}$ can in principle be based on reported experimental probabilistic distributions as in (65) whereas a unique value of $C_{n,min}$ of 3 representing a configuration equivalent to an indirect tensile strength tests (38,42) can be assigned to all clumps. Based on the above parameters, breakage is implemented by releasing selected spheres from the clump as a function of the acting normal contact force f_n , particle loading configuration, characterized by the clump coordination number C_n , and local contact geometry as follows:

- i. Corner breakage: this is the case for asperities when $f_n \geq f_{n,f}$. Corner breakage results in the sphere representing the asperity being released from the clump mimicking the breakage of angular projections, see Figure 18.

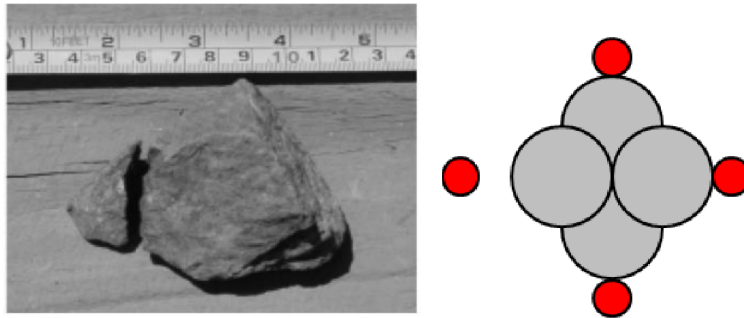


Figure 18. Example of corner breakage in ballast particle³ and DEM modelling.

- ii. Particle splitting: this is the case for spheres in the clump body when $f_n \geq f_{n,f}$ and $C_n \leq C_{n,min}$. Figure 19 shows an example of particle splitting in several parts, characterized by equal parts in two main different sizes. Following this, splitting is implemented by releasing all balls from the clump, resulting in two sizes: four main body balls and maximum four asperity balls (asperities may be less than four due to corner breakage during previous loading cycles).

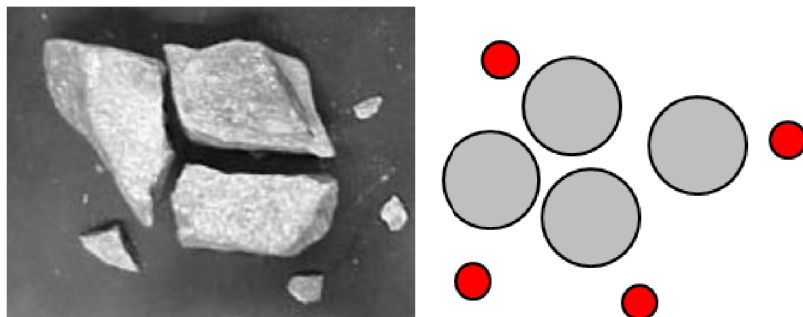


Figure 19. Example of particle splitting in ballast particle⁴ and DEM modelling.

³ Reprinted by permission from THOMAS/TELFORD LTD: ICE Publishing, *Géotechnique*, Effect of confining pressure on the degradation of ballast under cyclic loading, Indraratna B, Lackenby J, Christie D © 2005.

⁴ Reprinted by permission from: Springer Nature, *Granular Matter*, Discrete Element Method Analysis of Railtrack Ballast Degradation during Cyclic Loading, Lobo-Guerrero S, Vallejo LE © 2006.

The particles resulting from these processes could in principle be liable to further particle splitting as in (38). Given the challenges in computational time, splitting is limited to the primary one. In this regard, the aforementioned study where subsequent particle splitting was allowed resulted in no more than a third generation of crushing. Also, several studies indicate that although particle splitting is present in railway ballast materials, is not generally the dominating mechanism (40,41).

The introduced model presents several advantages when compared with previous state of the art efforts by Lu & McDowell (11,15) based on ten-ball tetrahedral clumps to which eight asperities were bonded. First and foremost, substantial gains in computational time as results of the use of simpler clumps and the avoidance of bonds. This allows not only to consider corner breakage but particle splitting too without a prohibitive computational costs as in (11,15). Secondly, breakage is controlled by fewer parameter, i.e. 3 parameters compared to 12 in (11,15), and with a much clearer physical meaning. Overall, it results in a more computationally efficient and robust model suitable for implementation in rockfill embankments.

3.2 Triaxial testing

Triaxial testing is mainly used for developing and testing the material model to be implemented for rockfill embankments. Triaxial testing is advantageous as (1) it allows to develop the material model in a much reduced scale compared to the whole embankment and under more controlled conditions and (2) it is well documented for ballast materials (41,42) allowing comparison with model results. A brief summary of the numerical procedures and main results is given in this thesis, as the focus is on rockfill embankments, see Section 3.3. More detailed information on triaxial testing can be found in Publication IV.

3.2.1 Numerical procedures

A semi-compacted mixture of tetrahedral clumps is generated by particle inflation within a frictionless cylindrical vessel based on the material-genesis algorithm described in (36). Basically, the material vessel is first filled with a packing of frictionless spheres with random placement, followed by relaxation and substitution for randomly oriented clumps. The main difference with the procedure in (36) is that inter-particle friction μ_g is added to the clumps at this point before further relaxation and stress installation. This controls the final porosity by hindering particle rearrangement and leading to a less compacted configuration. On completion of generation, the final friction coefficient μ is assigned to all

particles. The main input micromechanical properties for specimen generation are summarized in Table 8, where parameters are generally chosen in order to result in a scaled-up version of the tests in (11,15,41,66). Vessel dimensions are a compromise between computational time and size dependency of the system behaviour.

Table 8: Main input micromechanical parameters for triaxial specimen generation.

Property	Value
Particle size ratio $PSR = D_{\max}/D_{\min}$	1.2
Spherical particle minimum diameter D_{\min}	192 mm
Specimen height H_{spc}	3000 mm
Specimen diameter D_{spc}	1500 mm
Particle density ρ	2500 kg/m ³
Contact elastic modulus E_c	400 MPa
Particle normal to shear stiffness ratio k_n/k_s	1.0
Initial target stress p_0^\dagger	10 kPa
Particle friction coefficient during generation μ_g	0.06
Particle friction coefficient after generation μ	0.6

The specimen is then subjected to cyclic loading for a total of 500 load cycles (10 conditioning cycles followed by 490 full load cycles). The deviatoric stress is cycled between a minimum $\sigma_{d,\min}$ and maximum $\sigma_{d,\max}$ value under confinement pressures ranging between 60 and 240 kPa (see Table 9). These are selected within the range of the ones in the experimental tests in (41,66) with the lowest $\sigma_{d,\max}/\sigma_c$ ratios (see Section 1.3.2), as even lower ratios are anticipated for embankments. Monotonic loading until failure is also performed for the same confinement levels. The loading procedures are similar to the ones already described in Section 2.3 with a maximum axial strain rate of 0.005 s⁻¹ for the present case.

For the considered stress levels, a series of tests not including degradation, namely “unbreakable”, and another series including degradation, correspondently “breakable”, are performed for both monotonic and cyclic tests. Fracture loads $f_{n,u}$ are assigned to all balls by following the distribution in Figure 20 representative of experimental distributions for granite (65). The coordination number value above which particle splitting is inhibited $C_{n,min}$ is set to 3 in accordance with a configuration equivalent to an indirect tensile strength test (38,42).

Table 9: Stress levels for cyclic triaxial tests.

σ_c [kPa]	$\sigma_{d,min}$ [kPa]	$\sigma_{d,max}$ [kPa]	$\sigma_{d,max}/\sigma_c$
60	45	230	3.8
90	45	230	2.6
120	45	230	1.9
180	45	230	1.3
240	45	230	1.0

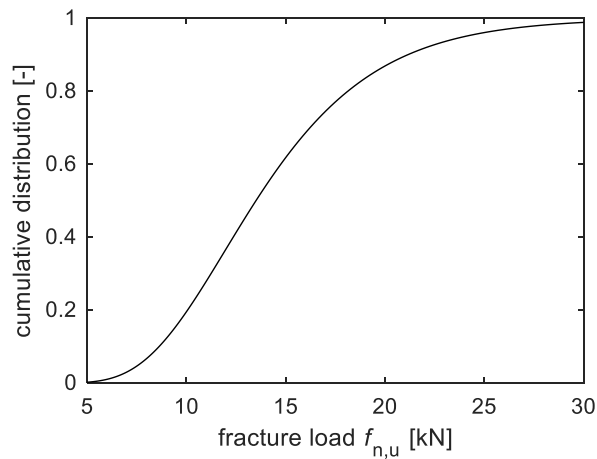


Figure 20. Distribution of fracture loads among balls in numerical specimens.

3.2.2 Main results and discussion

The main properties of the generated specimen are summarized in Table 10, where results from (11) also are included for comparison. A porosity value of 0.51 is obtained, close to the 0.49 in (11), but both numerical values higher than the ones for the laboratory specimens in (66) and (41), corresponding to monotonic respectively cyclic loading and overall ranging between 0.42 and 0.46. However, porosity is highly dependent on particle shape and hence numerical values should not directly be compared with the experimental ones. Regarding the numerical specimens, it can be seen that even though both studies have similar number of particles, the present study uses a significantly lower number of spheres, clearly resulting in significant reductions in computational time demands. Figure 21 allows to compare the PSD for the numerical mixture together with the experimental specimens, where it can be appreciated that the numerical mixture is a scaled-up version of the experimental PSDs. Considering the level of simplifications and uncertainties embedded in the model together with the reported high inconsistency on the effect of gradation scale on mechanical performance (52), numerical results are to be directly compared with the experimental ones. The generated specimen is shown in Figure 22.

Table 10: Triaxial specimen volumetrics after generation. Result for bonded model in (11) added for comparison.

Property	Value	Bonded model after (11)
Minimum particle equivalent diameter D_{\min}	220 mm	40 mm
Maximum particle equivalent diameter D_{\max}	264 mm	40 mm
Total number of spheres N_{sph}	4 899	11 124
Total number of clumps N_{cl} [-]	671	618
Initial porosity n_o [-]	0.51	0.49

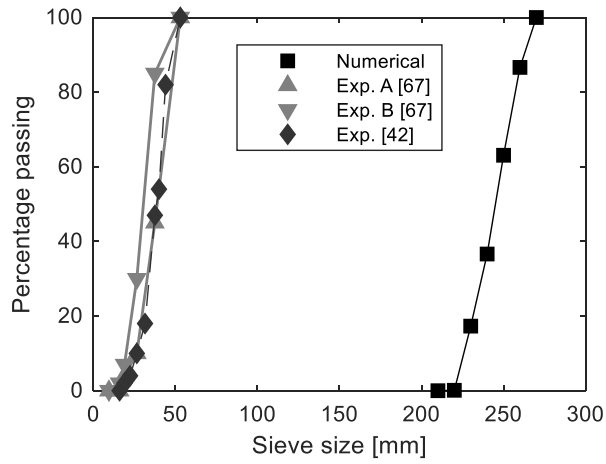


Figure 21: Numerical and experimental particle size distribution (PSD) for triaxial testing. Experimental (exp.) PSD after (66) for gradations exp. A and exp. B, and after (41).

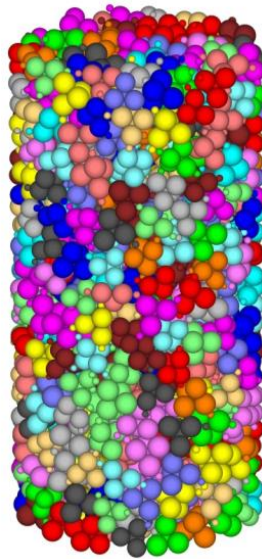


Figure 22: Numerical specimen for triaxial testing after generation. Different colours to indicate different clumps.

Regarding monotonic loading to failure, stress-strain diagrams, i.e. $\sigma_d(\varepsilon_a)$ diagrams, for numerical breakable and unbreakable assemblies are obtained and compared to the experimental results in (66). Comparison with the numerical results for the bonded DEM model in (11), trying to also replicate the tests in (66), is undertaken as well. Analogously, results for volumetric strain ε_v are obtained and compared with experimental and numerical ones. Degradation is shown to reduce shear strength and inhibit dilation, resulting in a significantly more realistic response. Compared to the bonded model, a higher level of resemblance in shear strength response is obtained with the proposed model. All diagrams can be consulted in Publication IV.

For the case of cyclic loading, numerical breakable specimens achieved shakedown in agreement with experimental results (41), with the only exception of the lowest confinement level. Shakedown took place at an accelerated rate for the numerical specimens (approximately after 100 load cycles out of 500, see Publication IV) whereas for the experimental tests this happened after approximately 10 000 cycles of the applied 50 000 cycles (41). This type of behaviour had already been observed in the bonded model too (11), where an even more rapid shakedown took place (in less than 10 cycles out of a total of 100 cycles). Rearrangement and degradation develop hence considerably faster in numerical specimens and it is hypothesized that a reduced number of load cycles could represent a larger one in reality (a ratio of approximately 1 to 100 is observed in this study). This is speculated to be partly caused by the chosen slow loading rate (see Section 3.2.1) that maximizes rearrangement under each load cycle. The limited number of large asperities and ignoring the effects of fatigue and slow crack growth have also been suggested as causes (11). Final axial and volumetric strains for breakable and unbreakable specimens together with experimental results (41) and result from the bonded model (11) are summarized in Figure 23 where all tests were cycled between deviatoric values of 45 kPa to 230 kPa. Degradation increases permanent strain and contractibility, resulting in considerably more realistic responses. Furthermore, breakable series show a higher degree of similarity to the experimental results than the previously proposed bonded model.

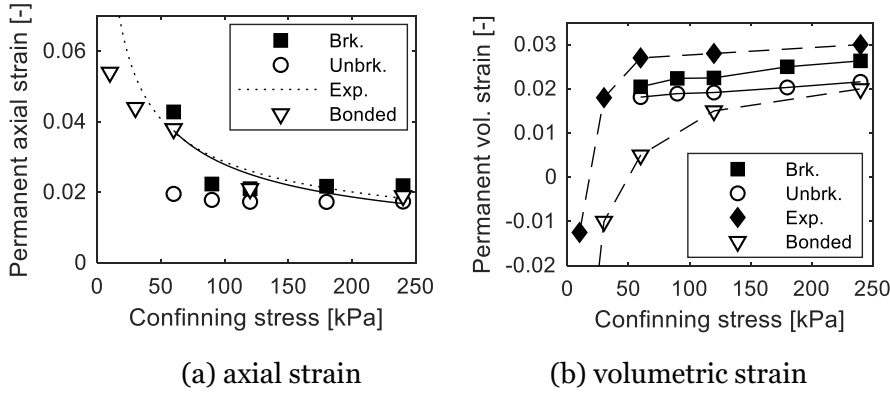


Figure 23: Effect of confinement on final permanent strains for (a) axial strains and (b) volumetric strains for unbreakable (Unbrk.), breakable (Brk.), experimental (41) (Exp.) and bonded model in (11) (Bonded) cyclic triaxial tests. Experimental tests results for axial strains in (a) represented by dotted regression line $\varepsilon_{a,p} = 0,30\sigma_c^{-0,51}$ following (41). Solid regression line of type $\varepsilon_{a,p} = a\sigma_c^{-b}$ added for breakable tests (Brk.) in (a).

Results regarding the resilient response, characterized by the resilient modulus, are summarized in Figure 24. Approximately linear stiffening of the modulus is observed for numerical specimens, in agreement with the experimental results (41). Good agreement between numerical and experimental values is appreciated for higher confinements, whereas for lower confinements the numerical results underestimate the experimental ones. The effect of breakage is much less pronounced than for the permanent strains, suggesting that breakage mainly influences the permanent part and has a lesser effect on the resilient component. It should be noted that the authors of Publication IV do not know of any other attempt on DEM modelling of granular materials under triaxial loading where both the permanent strain and resilient response are presented. The only exception may be combining Publication II and Publication III, however being these studies of a more behavioural nature as presented in Section 2.4.

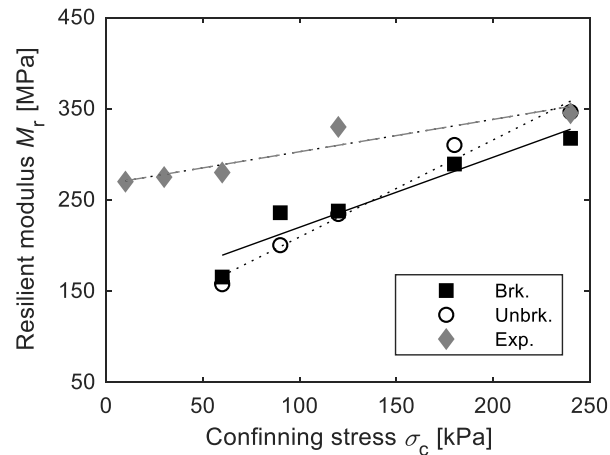


Figure 24. Effect of confinement on the final resilient modulus for breakable (Brk.), unbreakable (Unbrk.) and experimental (41) (Exp.) cyclic triaxial tests. Linear regression lines included as solid, dotted and dashed lines respectively.

Publication IV also investigates the influence of different processes and parameters at particle level on the macroscopic response. In particular, the effect of breakage is studied, concluding that corner breakage is dominant over particle splitting for all stress levels (see Figure 25), as expected for angular ballast materials (40,41) and explained by high coordination numbers. A distinct correlation between the development of corner breakage and permanent axial strain with loading cycles was also established in agreement with (11). Ultimately, it was shown that it is in fact a complex interdependency of factors at both particle and macroscopic level that explain the mechanical response of the breakable assemblies. Additionally, clear signs of stress history dependence were identified at particle level.

In summary, an efficient and robust model with at least a similar level of resemblance to empirical results as a previous state of the art bonded model (11) under a range of stress levels closer to those anticipated for embankments is presented in Publication IV. Its implementation to model high rockfill embankments is presented in Section 3.3, corresponding with Publication V. This implementation would be unthinkable in practical terms with the bonded model in (11).

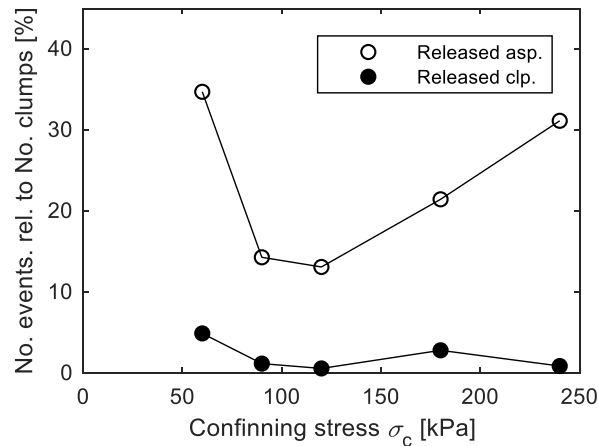


Figure 25. Degradation under cyclic triaxial loading for breakable tests. Released asperities (asp.) represent corner breakage whereas released clumps (clp.) represent particle splitting.

3.3 Embankment modelling

In this section, the breakable clumps presented and tested under triaxial conditions in Publication IV (see Section 3.2) are implemented on the modelling of high rockfill railway embankments. This part corresponds with Publication V.

3.3.1 Numerical procedure

A brief description of the procedures for embankment generation and loading implemented in PFC3D v4.0 (36) is presented below. More detailed information can be found in Publication V.

Following Section 3.2, particles consist of tetrahedral clumps with four asperities (Figure 17). Half-track rockfill embankment models are generated for rockfill heights H ranging from 2 to 10 m in steps of 1 m. Regarding the length of the model in the track direction, a four-sleeper model is chosen, equivalent to 2.6 m along the track (650 mm sleeper spacing assumed). Cross-section dimensions are based on Figure 5 for the considered rockfill heights. Overall cross-section dimensions for selected embankment models are summarized in Figure 26.

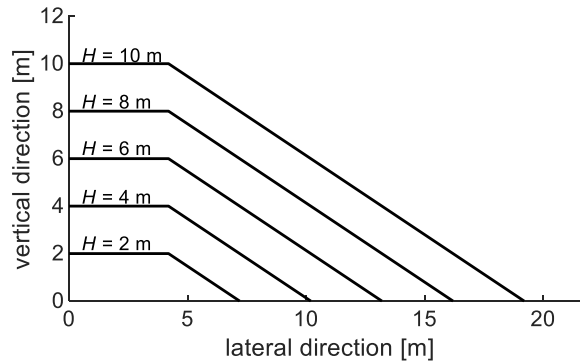


Figure 26. Overall cross-section dimensions for selected embankments. Lateral slope 2V:3H.

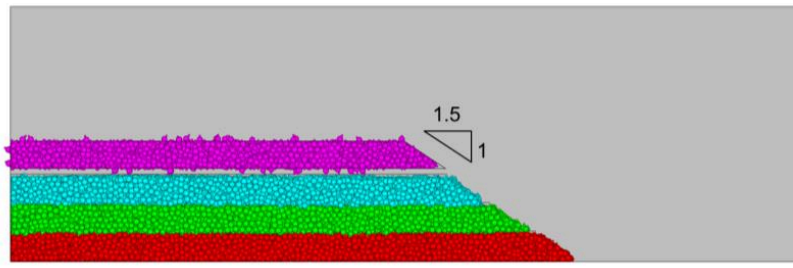
Micromechanical properties are generally chosen in accordance with Section 3.2. Vertical boundary planes (see Figure 27.b) are assigned with same stiffness and friction as the initial average particle values in order to represent the effect of the surrounding material on the modelled portion of the embankment. Same applies to the bottom wall representing the foundation. A summary of the main input micromechanical properties is presented in Table 11.

Table 11: Micromechanical input parameters for embankment generation

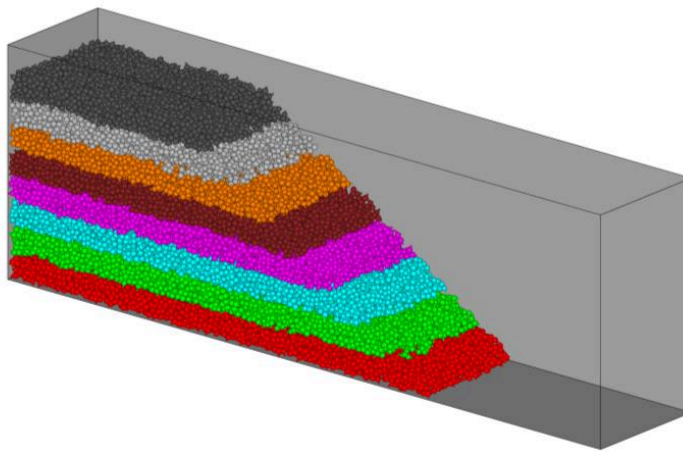
Property	Value
Particle size ratio $PSR = D_{max}/D_{min}$ [-]	1.2
Spherical particle minimum diameter D_{min} [mm]	160
Particle density ρ [kg/m ³]	2500
Contact elastic modulus E_c [MPa]	400
Particle friction coefficient μ [-]	0.6
Wall friction coefficient [-]	0.6

The main feature of the generation procedure is that embankments are constructed by successive dumping and compaction of layers of clumps on

top of each other until obtaining the desired compacted height. After generation of the overall boundary walls, a trapezoidal container for material dumping is generated (see Figure 27.a). For the first layer, the dumping container is at a distance of 0.1 m from the overall bottom boundary wall. For successive layers, this is generated at 0.1 m from the top of the latest compacted layer. The dumping container is filled with a collection of frictionless spheres at low porosity (0,5) following the PSD outlined in Table 11. The mixture is relaxed and balls are then substituted by clumps. After further relaxation of the assembly of clumps, particle friction is applied and the dumping container deleted allowing for free fall under gravity on top of the so far compacted rockfill.



(a)



(b)

Figure 27. Embankment generation for $H=4$ m: (a) front view of intermediate state prior to dumping of layer 4 and (b) three-dimensional view of final compacted embankment including boundary walls. Different clump colours indicate different rockfill layers.

Once the dumped layer has settled, a compacting wall is created right on top of the highest clump. The wall is progressively accelerated downwards to a selected maximum compacting velocity that is low enough to ensure substantial rearrangement. Once the chosen maximum normal compacting stress is achieved, the wall is halted to a stop and unloading proceeds in a similar fashion until the reaction force on the compacting wall is null. This loading-unloading procedure is repeated for the selected number of compaction cycles. Although the implemented compaction procedure is not expected to fully reproduce the compaction of real granular layers, it is nevertheless more realistic than other common generation techniques, such as those based on particle inflation (36) or the dynamic method (67), which have been implemented in the modelling of the railway ballast layer, e.g. (14). Table 12 summarizes the main input parameters defining the dumping and compaction procedures. Figure 27 showed an example of the embankment generation for $H = 4$ m, both for an intermediate stage and the final compacted embankment.

Table 12: Parameters for material dumping and layer compaction during embankment generation.

Property	Value
Thickness of dumping container $t_{\text{cont}}^{\text{p}}$ [m]	0.5
Dumping time [s]	1.0
Max. wall compaction velocity $v_{\text{max}}^{\text{c}}$ [m/s]	0.01
Max. compaction normal stress $\sigma_{\text{n}}^{\text{c}}$ [kPa]	100
Number of compaction cycles N_{c1}^{c} [-]	5

After generation, the embankment is loaded with a permanent load equivalent to the self-weight of the infrastructure above the granular layer (see Figure 5), estimated as roughly 25 kPa at the FPL/rockfill interface. Permanent loading is applied by a horizontal wall on top of the compacted embankment that is progressively accelerated up to a maximum chosen velocity. Once the permanent loading is fully applied, the wall is halted and the assembly allowed to relax. Then, a traffic cyclic load based on an axle load of 300 kN for heavier than normal rail traffic, resulting in approximately 13.5 kPa, is superimposed. Traffic loading is applied on top

of the permanent loading for a total of 500 load cycles (10 conditioning cycles followed by 490 full load cycles). The traffic loading-unloading cycle follows a similar procedure as for layer compaction during generation, i.e. progressive acceleration up to a chosen speed and once a maximum total normal stress of 38.5 kPa is achieved, the procedure is reversed until unloading back to 25 kPa. The main loading parameters are summarized in Table 13.

A series of test not including degradation, i.e. “unbreakable”, and a series including degradation, i.e. “breakable”, were performed, where degradation was activated on the onset of traffic loading. The parameters defining degradation were chosen according to the ones for triaxial testing (see Section 3.2.1).

Table 13: Parameters for embankment loading.

Property	Value
Width of loading wall in the lateral direction [m]	4.2
Friction coefficient of loading wall [-]	0.6
Max wall velocity at permanent loading v_{\max}^{PL} [m/s]	0.01
Max wall velocity at traffic loading v_{\max}^{TL} [m/s]	0.01
Normal stress at permanent loading σ_n^{PL} [kPa]	25.0
Normal stress at traffic loading σ_n^{TL} [kPa]	13.5

3.3.2 Main results and discussion

Table 14 summarizes the basic volumetric properties after generation. The number of clumps varies from less than 5 000 to more than 50 000, highlighting the tremendous computational time challenges associated with higher embankments. It can be seen that all embankments have almost identical particle sizes and that a slight decrease in porosity is observed with embankment height. The rest of this section will focus on results after embankment loading. More results and discussions concerning embankment compaction can be found in Publication V.

Table 14: Embankment volumetrics after generation.

Target height H [m]	Compacted height H_{emb} [m]	No. of layers [-]	No. of clumps [-]	Porosity [-]	Max. particle size [mm]
2,0	2.04	4	4 802	0.538	238.3
3,0	3.05	6	8 199	0.535	238.2
4,0	4.06	8	12 263	0.533	238.0
5,0	5.09	10	16 994	0.531	238.5
6,0	6.09	12	22 397	0.529	238.3
7,0	7.13	14	28 423	0.528	238.3
8,0	8.11	16	35 238	0.526	238.4
9,0	9.12	18	42 519	0.526	238.3
10,0	10.19	20	50 509	0.526	238.4

Settlements due to traffic loading are summarized in Figure 28 for both the breakable and unbreakable series. The lowest embankments seem to be unaffected by breakage. However, for intermediate and high embankments, breakage does result in a profound effect for half of the studied cases, and in one occasion even near doubling the settlements of the corresponding unbreakable assembly. Embankment height does not seem to influence settlements other than for the lowest embankments, where settlement initially diminish with embankment height. For intermediate to high embankment a substantial degree of variability is observed, indicative of the significant uncertainties associated with settlements prediction.

The evolution of settlement accumulation is presented in Figure 29 for selected embankments. Unlike triaxial behaviour as in Lackenby et al. (41), where all specimens reached shakedown, embankment settlements continue to grow. This can be attributed to the fundamentally different boundary conditions. Embankment settlements follow an initial phase of logarithmic growth after conditioning, something long observed for granular materials (68,69). After this phase, lasting for approximately 100

load cycles, some breakable tests continue the previous phase, whereas others switch to a new accelerated logarithmic growth. The type of behaviour seems to be independent of embankment height. For unbreakable tests, changes after the initial logarithmic growth are generally less dramatic. Nonetheless, some slight increase in growth rate is observed. Regarding the number of modelled cycles, it has been postulated in Section 3.2.2 that rearrangement and degradation develop considerably faster in numerical specimens and hence the number of modelled load cycles could represent a larger one in reality. Reasons for this were also suggested in Section 3.2.2.

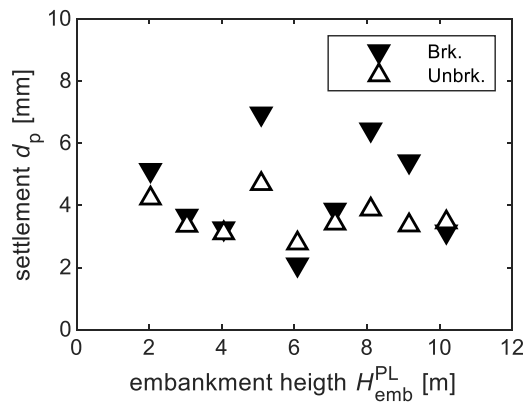


Figure 28. Embankment settlement due to traffic load for breakable (Brk.) and unbreakable (Unbrk.) assemblies.

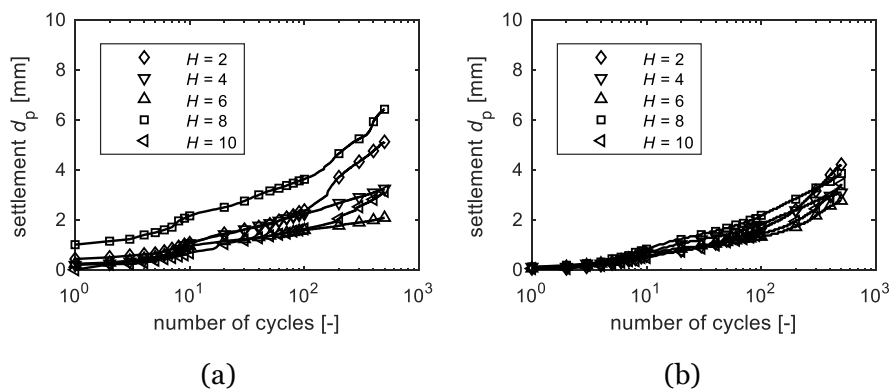


Figure 29. Embankment settlement evolution under traffic for (a) breakable and (b) unbreakable assemblies.

The resilient response on completion of traffic loading is presented in Figure 30. Linear stiffening with embankment height can be observed, as was the case for the triaxial tests with confinement (Section 3.2.2). In fact, close to lineal growth of the average lateral confinement with embankment height was also observed in Publication V. Degradation has a minor effect on the resilient response, as was again the case with triaxial tests (Section 3.2.2). Nevertheless, breakable assemblies are on average slightly stiffer than unbreakable ones. This can be explained by the low levels of degradation experienced by the embankments (see below) resulting in a beneficial slight densification as already pointed out in Section 3.1.1. This serves also as explanation on why, for very few cases, settlements for breakable embankments are smaller than for unbreakable ones (Figure 28). In these cases, it can be speculated that the beneficial stabilizing effect of breakage overcomes its potential for increasing settlements. Values of resilient moduli can be considered similar to rockfill moduli for well compacted dams after construction (34).

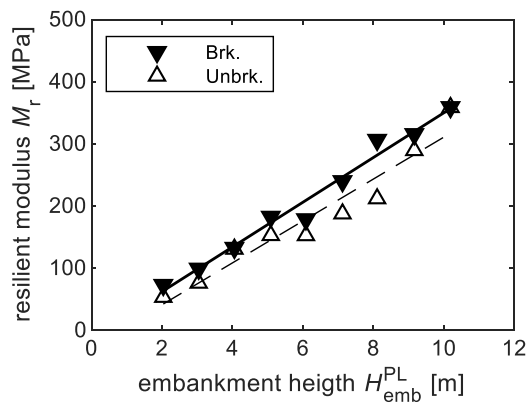


Figure 30. Embankment resilient response after traffic for breakable (Brk.) and unbreakable (Unbrk.) assemblies.

Regarding degradation, Figure 31 summarizes the final accumulated particle degradation for all breakable tests. Corner breakage is dominant in all cases, as was the case for the triaxial tests (Figure 25). Degradation values for embankments are more than one order of magnitude lower than for triaxial tests as result of lower stress levels. For triaxial tests, similarities between the evolution patterns of settlements and corner breakage were found. This was not the case for embankments (Publication V), which may be explained by their low levels of degradation. Lastly, an average oscillatory increase in degradation with embankment height is

observed. However, the highest values of degradation are for the lowest embankment. Explanations based on boundary effects and singularities on the contact forces network are presented in Publication V and supported by results at particle level.

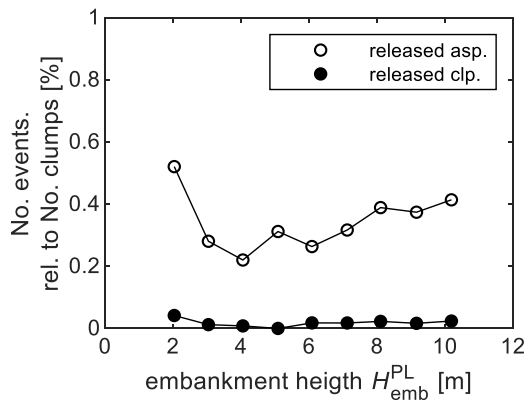


Figure 31. Embankment particle degradation after traffic.

Results at particle level were used in Publication V to provide explanation to some of the observed behaviours. In particular, the lack of effect of embankment height on settlements for intermediate and high embankments was investigated. It was shown that, although the average lateral confinement did grow with embankment height and therefore should result in lower settlements, local confinement of the top layers was rather unaffected. It was also shown, based on the distribution of particle rotational velocities as an indicator of particle rearrangement, that settlements were concentrated in the top layers, and hence did not benefit from the added average confinement, therefore providing an explanation to the apparent lack of influence of embankment height and corresponding average lateral confinement. A more detailed explanation follows.

Figure 32 shows the distribution of particle angular velocities, represented by their modulus, at the end of the last unloading cycle for selected embankments. Rotational velocities follow similar distributions when considering the top four layers, i.e. ca. the top two meters. When the whole embankment is considered, distinctive variation between embankments are observed. For these, rotations decrease with embankment height, especially for lower embankments, becoming this decrease smaller for higher embankments. This can be explained by the fact that the deeper within the embankment, the less rotation is produced

by loading of the top layer (comparison of results for top layers, i.e. Figure 32.b and the whole embankment, i.e. Figure 32.a, supports this explanation). Therefore, for high embankments, the more inert part dominates the average values, whereas for low embankment, the top layers still represent a substantial part of the body of the embankment and hence dictate the average values (compare results for top layers and whole embankment for $H=10$ m and $H=2$ m). All this supports the assumption that rearrangement under traffic concentrates on the top layers and explains the lack of effect of embankment height on settlements, especially for intermediate to high embankments. It is therefore this substantial scale difference with triaxial conditions that ultimately seems to dictate the observed discrepancies on the effect of confinement on settlements.

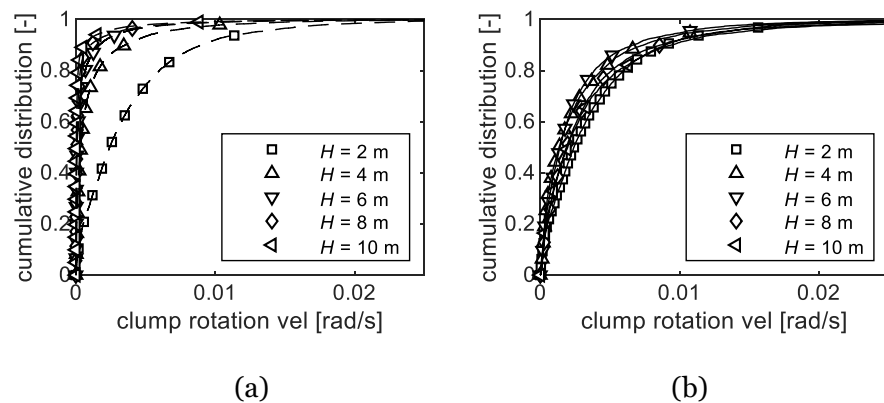


Figure 32. Distribution of particle rotation velocities for breakable tests: (a) the whole embankment and (b) the top four layers.

Figure 33 provides additional information on the spatial distribution of breakage not included in Publication V. The cumulative distribution of breakage events, i.e. both corner breakage and particle splitting, with embankment height is shown for all the studied embankments. An initial linear growth can be observed for all embankments. This develops into a non-linearity for the highest portion of the embankment as a result of a deceleration in breakage growth. This final non-linearity is more noticeable the higher the embankment is. The initial linear growth for the bottom half of the embankment is consistent with a homogeneous distribution of breakage, assuming a certain balance between the embankment slope and the load spreading effect of the granular fill. The reduction in cumulative breakage growth with height for the top half, i.e. the non-linearity, indicates that contact forces are lower in a zone where

the opposite may have been anticipated due to: (1) being closer to the applied traffic load and (2) with a lesser horizontal area for load distribution albeit of the embankment slope. It should also be observed that locked stresses grow the deeper within the embankment fill as a result of the successive compaction of layers on top of each other during generation (see Publication V). Altogether, this suggests that, for the considered compaction procedure and loading conditions, locked stress levels resulting from embankment compaction play a greater role than traffic loading in inducing breakage.

In particular, Figure 34 shows the location of the spheres released from the clumps, i.e. resulting from corner breakage and particle splitting, for the 10 m high embankment. Blue spheres represent the ones where the maximum acting contact normal force was lower than the assigned fracture load. These correspond with particle splitting for spheres other than the one in the clump body where the contact force exceeded the fracture load. The latter type of spheres together with released asperities resulting from corner breakage are shown by the smaller red dots. A more or less uniform distribution over the bottom half of the embankment is observed in agreement with Figure 33. For the top half, a reduction in breakage density takes place. Additionally, reduced breakage near the free slope and a certain concentration of breakage at the very top of the embankment, i.e. directly under the loading wall, are also observed, as could have been anticipated.

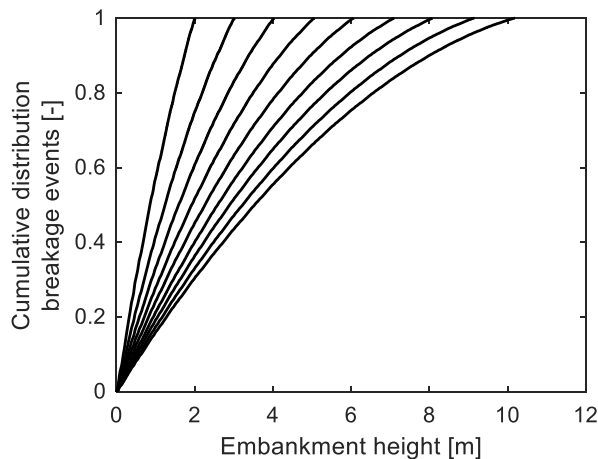


Figure 33. Cumulative distribution of breakage with embankment height. Presented lines correspond to total embankment heights ranging from 2 to 10 m in 1 m steps from left to right.

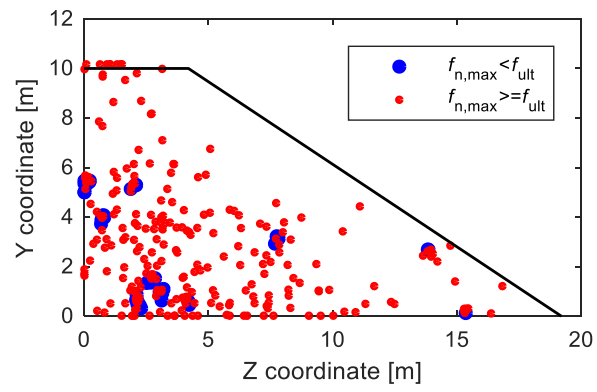


Figure 34. Spatial distribution of spheres resulting from breakage, i.e. released from clumps, for $H=10$ m.

4. Concluding remarks and further research

In this final chapter, the main conclusions of the work are presented highlighting the scientific contribution to the *status quo*. Furthermore, suggestions for further research on high rockfill embankments using DEM are given.

4.1 Concluding remarks

The work presented in this thesis has shown some of the capabilities of DEM to gain insight into the micromechanical processes governing the behaviour of granular materials. Specifically:

- The first part of the work, of a more theoretical nature, has been centred on perfect binary mixtures of elastic spheres. The load-bearing fabric of the numerical mixtures has been characterized based on results at particulate level and its significance on macroscopic performance assessed. Behavioural similarities with granular materials have also been established, meaning that results and conclusions for the numerical mixtures can partly be extrapolated to real granular mixtures.
- On the second part of the work, of a more applied nature, high rockfill railway embankments are studied with certain emphasis on slab-track configurations. Non-spherical particle shape and particle degradation are explicitly accounted for in the material model, resulting in a more realistic modelling attempt. The model is used to study the influence of embankment height and different processes at particle level, like particle breakage, on the macroscopic mechanical response of the embankment to cyclic loading induced by traffic.

4.1.1 Soil fabric

The effect of fines content on the force transmission at particulate level under triaxial loading was initially studied and results used to define a load-bearing fabric classification system in accordance with existing systems. The main scientific contribution of the new system is that the role of coarse and fine components are explicitly quantified in terms of force transmission rather than inferred from the macroscopic response or different volumetric indices as in previous studies. The proposed system has been shown to be fairly robust to variations in stress levels and a good predictor of the relative macroscopic performance of the assemblies. In this regard, it must be observed that the proposed fabric classification

system was based exclusively on micromechanical considerations regarding force transmission at particulate level without any consideration to macroscopic performance aspects. Nevertheless, a good correlation between soil fabric and performance could be established. Generally, higher resilient modulus and lower permanent strain were observed for interactive fabrics, whereas the opposite held for instable fabrics. Explanations and methods for identifying instability have been proposed.

Numerical assemblies also showed good agreement with empirically-based relations characterizing the stress dependency of the resilient modulus and permanent deformation for granular materials. In particular, it was found a strong dependence of the resilient modulus with the confinement to deviator stress ratio whereas permanent deformation was also influenced by the stress path length; furthermore, the permanent deformation could be explained by stress path closeness to failure in accordance with existing models used in pavement engineering. These similarities support using numerical mixtures, even in their simpler expression, to provide insight into the processes at particulate level that explain granular behaviour in general and, in particular, into the effects of soil fabric structure on the macroscopic performance of granular materials for pavement and railway applications.

4.1.2 Rockfill embankments

A DEM material model suitable for its implementation in large constructions of unbound stone-based materials was firstly developed and tested under triaxial conditions. Particles were based on simple tetrahedral breakable clumps. Both corner breakage and particle splitting were included, where breakage processes were controlled by values of contact forces, coordination number and the local contact geometry. Results were compared against railway ballast experimental and numerical state of the art modelling results, for different triaxial tests types and multiple measurements types, under a range of stress levels closer to those anticipated for embankments. It was shown that the proposed model resulted in an efficient and robust model with nevertheless a comparable degree of similarity to empirical results as the previous modelling effort. Among some of the most significant conclusions, degradation was key in obtaining a realistic plastic response, by largely inhibiting dilation and increasing settlements, whereas its influence on the resilient response was much less pronounced. Different micromechanical parameters were used to explain the observed deformations. Breakage resulted in substantial changes in the evolution of these parameters and their effect on performance, resulting in none of these fully explaining the observed behaviour. In fact, a complex interdependency of factors at both particle

and macroscopic level could ultimately explain the behaviour of the breakable assemblies.

Subsequently the developed breakable clumps were implemented in the actual modelling of rockfill railway embankments, something not attempted before. Embankments with heights ranging between approximately 2 and 10 m were generated by successive dumping and compaction of layers of clumps on top of each other, mimicking the construction of real embankments. Cyclic loading of the embankments was undertaken for both breakable and unbreakable assemblies. Settlements did not generally seem to follow a discernible pattern with embankment height, especially for intermediate and high embankments. However, a clear effect of degradation was observed, largely resulting in increased settlements. An analysis of particle rotation velocities suggested that particle rearrangement and hence settlement accumulates mainly in the top layers, thus explaining the above behaviour. Regarding the resilient response, a linear stiffening effect of embankment height was observed with a minor influence of breakage. The key contribution is thus the modelling of high rockfill embankments including degradation, something not attempted before, where furthermore the construction process for real embankments is partly accounted for during embankment generation. Among the main conclusions is that the specific scale, boundary and stress conditions of embankments results in a behaviour deviating from that observed for ballast materials under triaxial conditions. Furthermore, the mechanical response is marked by a substantial degree of uncertainty that can be exacerbated by particle degradation.

Despite the numerous simplifications and limitations embedded in the embankment model, this is still deemed as a suitable tool to assess the order of magnitude of macroscopic responses and their relative evolution together with the relative level of significance of influencing factors. The model is especially advantageous in a field lacking full-scale measurements and moreover can be used to suggest explanations at particle level which experimental testing alone will fail to provide.

4.2 Further research

The lack of studies on full-scale measurements of settlements for rockfill railway embankments has been mentioned. Although empirical studies alone would fail to provide explanations at particle level for the observed macroscopic responses, complemented with numerical DEM modelling, these offer the potential for great micromechanical insight. Comparison of full-scale results with the numerical macroscopic behaviour can be used to validate the explanations at particle level obtained with DEM, which empirical testing alone fail to provide.

4.2.1 Material model and embankment generation

The use of relatively simple clumps of spheres to represent crushed rock particles has been argued and deemed necessary⁵ to deal with the great challenges in computational time. Even though complex clumps might be out of the question at the present moment, other aspects concerning simpler clumps can be investigated. For example, considering the present study, variation of the relative size of the asperities compared with the spheres constituting the body of the clump. Alternative, simple clumps other than the tetrahedral ones used in this study can be tested. Furthermore, the combination of different types of simple clumps could be easily implemented, e.g. (43). Additionally, a wider range of overall clump sizes could be used, representing more continuous gradations or even gap-graded gradations instead, in order to also study possible gradation effects. All of the above should be considered within certain practical restrictions in order to limit the number of involved particles and hence keep computational time needs within reasonable limits.

The implemented generation procedure consisting in dumping and compaction of layers of clumps on top of each other is not expected to fully reproduce the compaction of real granular layers, but nevertheless more realistic than other common generation techniques. The purpose was to develop a procedure resulting in a similar level of compaction and locked internal stresses as a compacted granular layer. More realistic compaction techniques could be implemented, like compaction by a rolling cylindrical wall, expected to resemble in a greater degree compaction rollers. Furthermore, independently of the selected modelling technique, the effect of compaction effort, characterized by, among other fundamental parameters, the number of passes and lift thickness on the final resistance to settlement accumulation under traffic loading may be investigated. In fact, compaction of embankments for transport infrastructures is a current topic of research, e.g. (70,71).

Following with the compaction procedure, breakage was not included during generation. This was done to limit computational time during embankment generation. However, it has been shown in this thesis that most of the breakage is associated with the high levels of locked stresses in the deeper layers of the embankment as a result of compaction of the layers above. Therefore, inclusion of breakage during generation may be

⁵ Not only necessary, but it has been argued throughout this thesis as even adequate and sufficient given the lower stress levels in the rockfill and the developing of the material model with inclusion of breakage and comparison of results with different tests types and multiple measurements (see for example Section 1.3).

considered and results after loading compared with the ones obtained when omitting breakage during generation.

Regarding the degradation algorithm presented in this thesis, particle attrition was omitted. The algorithm focusses exclusively on those processes that can easily be explicitly included when representing particles by simple clumps of spheres, i.e. corner breakage and particle splitting. Nonetheless, given the relatively low amounts of breakage for embankments albeit of the low stress levels, the significance of attrition may need to be investigated. However, at the present time, the author is unable to suggest a way to explicitly include this process in the material model. A compromise on using a more implicit method like bonds (11,15) or a newly developed method to account for this process may be imperative if the process is to be accounted for.

4.2.2 Embankment loading

It has also been shown that rearrangement and degradation develop considerably faster in numerical specimens. This is in fact advantageous considering computational time limitations. The chosen slow loading rate together with the limited number of large asperities and ignoring the effects of fatigue and slow crack growth were suggested as causes in agreement with previous studies. This hypothesis could be investigated for intermediate embankments or under triaxial conditions partly to understand how these would influence the relative development of settlements other than by slowing down the process. However, great challenges in computational time should be expected.

Possible long-term settlements due to creep within the rockfill mass have not specifically been targeted in this study. The focus has been on settlements due to cyclic loading. The significance of creep on its own may also be investigated by subjecting the embankments to exclusively the permanent loading of the infrastructure above, other than the self-weight of the embankment itself. The relative importance of creep compared to traffic induced settlements may be investigated. Its relative evolution in time may also be studied, however comparison of its evolution with the number of applied load cycles or in absolute terms may prove to be troublesome. None of the above processes are studied in absolute terms when it comes to time, and the relative time scales may be of different nature.

Finally, partly connecting with the above presented suggestion on gradations and with the other main topic of this thesis, i.e. soil fabric of binary mixtures, the effect of fine particles on fabric and performance may be investigated. However, two questions should be considered carefully. First, the formulation presented in Section 2.1 is intended for spherical particles and not directly applicable to clumps. Secondly, fine spherical

particles in this study on embankments are the result of particle breakage. This means that their effect on performance is mainly the results of the breakage itself, unlocking added potential for particle rearrangement in the process and a corresponding potential for densification or loosening. This is far from the intended focus on the soil fabric investigation when considering the effect of fine particles on force transmission and performance. Unbreakable assemblies with certain contents of fine particles (spherical or otherwise the later) is suggested as a starting point in order to initially facilitate the study of soil fabric independently of breakage, as the later is expected to significantly influence the soil fabric as it has been the case with numerous micromechanical parameters and processes (see Publications IV and V).

References

1. European Aggregates Association. *UEPG Annual Review 2017-2018*. 2018.
2. Sveriges geologiska undersökning. *Grus, sand och krossberg 2017*. 2018.
3. Seed HB, CHAN CK, Lee CE. Resilience characteristics of subgrade soils and their relation to fatigue failures in asphalt pavements. *Proc. Int. Conf. Structural Design of Asphalt Pavements*. University of Michigan, Ann Arbor; 1962. p. 77–113.
4. Lekarp F, Isacsson U, Dawson A. State of the art. I: Resilient response of unbound aggregates. *Journal of Transportation Engineering*. 2000;126(1): 66–75.
5. Lekarp F, Isacsson U, Dawson A. State of the art. II: Permanent strain response of unbound aggregates. *Journal of Transportation Engineering*. [Online] 2000;126(1): 76–83. Available from: doi:10.1061/(ASCE)0733-947X(2000)126:1(76)
6. Terzaghi K. Old earth-pressure theories and new test results. *Engineering News-Record*. 1920;85(14): 632–637.
7. Rowe PW. The stress-dilatancy relation for static equilibrium of an assembly of particles in contact. *Proceedings of the Royal Society A: Mathematical, Physical and Engineering Sciences*. 1962;269(1339): 500–527.
8. Esveld C. Track requirements. *Modern Railway Track*. 2nd ed. Zaltbommel, the Netherlands: MRT-Productions; 2001. p. 13–14.
9. Cundall PA. A computer model for simulating progressive large scale movements in blocky rock systems. *Proc. Symp. Int. Rock Mech., Vol. 2, no. 8*. ISRM; 1971.
10. Cundall PA, Strack ODL. A discrete numerical model for granular assemblies. *Géotechnique*. Thomas Telford Ltd; 1979;29(1): 47–65.
11. Lu M, McDowell GR. Discrete element modelling of railway ballast under monotonic and cyclic triaxial loading. *Géotechnique*. [Online] 2010;60(6): 459–467. Available from: doi:10.1680/geot.2010.60.6.459
12. Yohannes B, Tan D, Khazanovich L, Hill KM. Mechanistic modelling of tests of unbound granular materials. *International Journal of Pavement Engineering*. Taylor and Francis Ltd.; 2014;15(7): 584–598.
13. Bian X, Huang H, Tutumluer E, Gao Y. “Critical particle size” and ballast gradation studied by discrete element modeling. *Transportation Geotechnics*. Elsevier Ltd; 2016;6: 38–44.
14. Liu Y, Deng A, Jaksa M. Three-dimensional modeling of geocell-reinforced

- straight and curved ballast embankments. *Computers and Geotechnics*. [Online] 2018;102: 53–65. Available from: doi:10.1016/j.compgeo.2018.05.011
15. Lu M, McDowell GR. Discrete element modelling of railway ballast under triaxial conditions. *Geomechanics and Geoengineering*. [Online] 2008;3(4): 257–270. Available from: doi:10.1080/17486020802485289
 16. Loganathan N, de Silva S, Thurairajah A. Strength correlation factor for residual soils. *Journal of geotechnical engineering*. American Society of Civil Engineers; 1992;118(4): 593–610.
 17. Vallejo LE, Mawby R. Porosity influence on the shear strength of granular material-clay mixtures. *Engineering Geology*. 2000;58(2): 125–136.
 18. Xu W-J, Hu R-L, Tan R-J. Some geomechanical properties of soil-rock mixtures in the Hutiao Gorge area, China. *Géotechnique*. 2007;57(3): 255–264.
 19. Xu W-J, Xu Q, Hu R-L. Study on the shear strength of soil-rock mixture by large scale direct shear test. *International Journal of Rock Mechanics and Mining Sciences*. 2011;48(8): 1235–1247.
 20. Jiang X, Cui P, Ge Y. Effects of fines on the strength characteristics of mixtures. *Engineering Geology*. 2015;198: 78–86.
 21. European Asphalt Pavement Association (EAPA). *Heavy duty surfaces: the argument for SMA*. Breukelen, The Netherlands: EAPA; 1988.
 22. Schmiedlin RB. Stone matrix asphalt: the Wisconsin experience. *Transportation Research Record*. [Online] Transportation Research Board of the National Academies; 1998;(1616): 34–41. Available from: <http://trrjournalonline.trb.org/doi/10.3141/1616-06>
 23. National Asphalt Pavement Association (NAPA). *Designing and constructing SMA mixtures – state-of-the-practice, Quality Improvement Series 122*. Lanham, MD, USA: National Asphalt Pavement Association; 1999.
 24. Indraratna B, Khabbaz MH, Salim W, Lackenby J, Christie D. Ballast characteristics and the effect of geosynthetics on rail track deformation. *International Conference on Geosynthetics and Geoenvironmental Engineering*. Bombay, India: Quest Publications; 2004. p. 3–12.
 25. The Concrete Countertop Institute. *The role of aggregate in concrete countertop mix designs*. [Online] Available from: <https://concretecountertopinstitute.com/free-training/the-role-of-aggregate-in-concrete-countertop-mix-designs/> [Accessed: 5th July 2019]
 26. Guarin A, Roque R, Kim S, Sirin O. Disruption factor of asphalt mixtures. *International Journal of Pavement Engineering*. [Online] 2013;14(5): 472–485. Available from: <http://www.scopus.com/inward/record.url?eid=2-s2.0-84873579854&partnerID=tZotx3y1>

27. Yideti TF, Birgisson B, Jelagin D, Guarin A. Packing theory-based framework to evaluate permanent deformation of unbound granular materials. *International Journal of Pavement Engineering*. 2013;14(3): 309–320.
28. Vallejo LE. Interpretation of the limits in shear strength in binary granular mixtures. *Canadian Geotechnical Journal*. 2001;38(5): 1097–1104.
29. Thevanayagam S, Shenthan T, Mohan S, Liang J. Undrained fragility of clean sands, silty sands, and sandy silts. *Journal of Geotechnical and Geoenvironmental Engineering*. 2002;128(10): 849–859.
30. Korkiala-Tanttu L. A new material model for permanent deformations in pavements. In: Horvli I (ed.) *Proc. of the Seventh Conference on Bearing Capacity of Roads and Airfields*. Oslo, Norway: Ny Media AS; 2005.
31. Momoya Y, Takahashi T, Nakamura T. A study on the deformation characteristics of ballasted track at structural transition zone by multi-actuator moving loading test apparatus. *Transportation Geotechnics*. [Online] Elsevier Ltd; 2016;6: 123–134. Available from: doi:10.1016/j.trgeo.2015.11.001
32. Al Shaer A, Duhamel D, Sab K, Foret G, Schmitt L. Experimental settlement and dynamic behavior of a portion of ballasted railway track under high speed trains. *Journal of Sound and Vibration*. [Online] 2008;316(1–5): 211–233. Available from: doi:10.1016/j.jsv.2008.02.055
33. Dascal O. Postconstruction deformations of rockfill dams. *Journal of Geotechnical Engineering*. [Online] 1987;113(1): 46–59. Available from: doi:10.1061/(ASCE)0733-9410(1987)113:1(46)
34. Hunter G, Fell R. Rockfill Modulus and Settlement of Concrete Face Rockfill Dams. *Journal of Geotechnical and Geoenvironmental Engineering*. [Online] 2003;129(10): 909–917. Available from: doi:10.1061/(ASCE)1090-0241(2003)129:10(909)
35. Clements RP. Post Construction Deformation of Rockfill Dams. *Journal of Geotechnical Engineering*. [Online] 1984;110(7): 821–840. Available from: doi:10.1061/(ASCE)0733-9410(1984)110:7(821)
36. Itasca Consulting Group Inc. *Particle Flow Code in 3 Dimensions (PFC3D) v4.0*. Minneapolis, USA: Itasca Consulting Group Inc.; 2008.
37. Lu M, McDowell GR. The importance of modelling ballast particle shape in the discrete element method. *Granular Matter*. [Online] 2007;9(1–2): 69–80. Available from: doi:10.1007/s10035-006-0021-3
38. Lobo-Guerrero S, Vallejo LE. Discrete element method analysis of railtrack ballast degradation during cyclic loading. *Granular Matter*. [Online] 2006;8(3–4): 195–204. Available from: doi:10.1007/s10035-006-0006-2
39. Suhr B, Marschnig S, Six K. Comparison of two different types of railway ballast in compression and direct shear tests: experimental results and DEM model validation. *Granular Matter*. [Online] Springer New York LLC;

- 2018;20(4). Available from: doi:10.1007/s10035-018-0843-9
40. Indraratna B, Lackenby J, Christie D. Effect of confining pressure on the degradation of ballast under cyclic loading. *Géotechnique*. [Online] 2005;55(4): 325–328. Available from: doi:10.1680/geot.55.4.325.65490
 41. Lackenby J, Indraratna B, McDowell GR, Christie D. Effect of confining pressure on ballast degradation and deformation under cyclic triaxial loading. *Géotechnique*. [Online] 2007;57(6): 527–536. Available from: doi:10.1680/geot.2007.57.6.527
 42. Lobo-Guerrero S, Vallejo LE. Visualization of crushing evolution in granular materials under compression using DEM. *International Journal of Geomechanics*. [Online] 2006;6(3): 195–200. Available from: doi:10.1061/(ASCE)1532-3641(2006)6:3(195)
 43. Hossain Z, Indraratna B, Darve F, Thakur PK. DEM analysis of angular ballast breakage under cyclic loading. *Geomechanics and Geoengineering*. [Online] 2007;2(3): 175–181. Available from: doi:10.1080/17486020701474962
 44. Lees G, Kennedy CK. Quality, shape and degradation of aggregates. *Quarterly Journal of Engineering Geology*. [Online] 1975;8(3). Available from: doi:10.1144/GSL.QJEG.1975.008.03.03
 45. Liu Y, Deng A, Jaksa MB. Discrete element modelling of geocell-reinforced track ballast under static and cyclic loading. *The 12th Australia–New Zealand Conference on Geomechanics Zealand Conference on Geomechanics*. [Online] Wellington; 2015. p. 279–286. Available from: https://www.researchgate.net/profile/Mark_Jaksa/publication/274421270_Discrete_Element_Modelling_of_Geocell-Reinforced_Track_Ballast_Under_Static_and_Cyclic_Loading/links/551fd6fc0cf2a2d9e140a234.pdf [Accessed: 15th December 2017]
 46. Huang H, Tutumluer E. Discrete Element Modeling for fouled railroad ballast. *Construction and Building Materials*. [Online] 2011;25(8): 3306–3312. Available from: doi:10.1016/j.conbuildmat.2011.03.019
 47. Selig ET, Waters JM. *Track geotechnology and substructure management*. London, UK: Thomas Telford Ltd; 1994.
 48. Branschsamverkan i grunden (BIG). *Höghastighetsspår i Sverige - på bank*. 2015.
 49. Thornton C, Zhang L. On the evolution of stress and microstructure during general 3D deviatoric straining of granular media. *Géotechnique*. 2010;60(5): 333–341.
 50. Minh NH, Cheng YP, Thornton C. Strong force networks in granular mixtures. *Granular Matter*. 2014;16(1): 69–78.
 51. Krishna P, Pandey D. Close-packed structures. In: Taylor CA (ed.) *International union of crystallography commission on crystallographic teaching, first series pamphlets, no. 5*. Cardiff, Wales: University College

- Cardiff Press; 1981. p. 1–4.
52. Lekarp F, Isacsson U. The effects of grading scale on repeated load triaxial test results. *International Journal of Pavement Engineering*. [Online] Taylor & Francis Group; 2001;2(2): 85–101. Available from: doi:10.3141/2154-15
 53. Ekblad J, Isacsson U. Influence of water on resilient properties of coarse granular materials. *Road Materials and Pavement Design*. 2006;7(3): 369–404.
 54. Song C, Wang P, Makse HA. A phase diagram for jammed matter. *Nature*. Nature Publishing Group; 2008;453(7195): 629–632.
 55. Dunlap WA. *A report on a mathematical model describing the deformation characteristics of granular materials*. Texas Transportation Institute (ed.) Texas A&M University; 1963. 1–44 p.
 56. Pezo RF. A general method of reporting resilient modulus tests of soils - A pavement engineer's point of view. *72nd Annu. Meeting of the TRB*. Washington, D.C.; 1993.
 57. Uzan J. Characterization of granular material. *Transportation Research Record*. Transportation Research Board; 1985;1022: 52–59.
 58. Morgan JR. The response of granular materials to repeated loading. *Australian Road Research Board Proc*. Vermont South, Australia: ARRB Group; 1966. p. 1178–1192.
 59. Brown SF, Hyde AFL. Significance of cyclic confining stress in repeated-load triaxial testing of granular material. *Transportation Research Record*. 1975;(537): 49–58.
 60. Knutson RM. *Factors influencing the repeated load behaviour of railway ballast*. University of Illinois at Urbana-Champaign, USA; 1976.
 61. Pappin JW. *Characteristics of granular material for pavement analysis*. University of Nottingham, UK; 1979.
 62. Lekarp F, Dawson A. Modelling permanent deformation behaviour of unbound granular materials. *Construction and Building Materials*. 1998;12(1): 9–18.
 63. McDowell GR, Bolton MD, Robertson D. The fractal crushing of granular materials. *Journal of the Mechanics and Physics of Solids*. [Online] 1996;44(12): 2079–2102. Available from: doi:10.1016/S0022-5096(96)00058-0 [Accessed: 21st April 2017]
 64. Lackenby J. *Triaxial Behaviour of Ballast and the Role of Confining Pressure under Cyclic Loading*. [Australia]: University of Wollongong; 2006.
 65. Celma Cervera C, Jelagin D, Partl MN, Larsson P-L. Contact-induced deformation and damage of rocks used in pavement materials. *Materials and Design*. [Online] 2017;133. Available from:

doi:10.1016/j.matdes.2017.08.003

66. Indraratna B, Ionescu D, Christie HD. Shear behavior of railway ballast based on large-scale triaxial tests. *Journal of Geotechnical and Geoenvironmental Engineering*. [Online] 1998;124(5): 439–449. Available from: doi:10.1061/(ASCE)1090-0241(1998)124:5(439)
67. McDowell GR, Harireche O, Konietzky H, Brown SF, Thom NH. Discrete element modelling of geogrid-reinforced aggregates. *Proceedings of the ICE - Geotechnical Engineering*. [Online] 2006;159(1): 35–48. Available from: doi:10.1680/geng.2006.159.1.35
68. Barksdale RD. Laboratory evaluation of rutting in base course materials. *Third International Conference on the Structural Design of Asphalt Pavements*. London, UK; 1972. p. 161–174.
69. Shenton MJ. Deformation of railway ballast under repeated loading conditions. In: Kerr AD (ed.) *Railroad Track Mechanics and Technology*. [Online] Princeton, New Jersey: Elsevier; 1978. p. 405–425. Available from: doi:10.1016/b978-0-08-021923-3.50025-5
70. Wersäll C, Nordfelt I, Larsson S. Soil compaction by vibratory roller with variable frequency. *Géotechnique*. [Online] 2016;67(3): 272–278. Available from: doi:10.1680/jgeot.16.p.051 [Accessed: 3rd May 2019]
71. Wersäll C, Nordfelt I, Larsson S. Resonant roller compaction of gravel in full-scale tests. *Transportation Geotechnics*. [Online] Elsevier Ltd; 2018;14: 93–97. Available from: doi:10.1016/j.trgeo.2017.11.004
72. Plato. *The Republic*. London, UK: Penguin Books Ltd; 1955.

Erratum (Publication IV)

de Frias Lopez R, Larsson S, Silfwerbrand J.

A discrete element material model including particle degradation suitable for rockfill embankments.

Computers and Geotechnics. [Online] Elsevier Ltd; 2019;115.

Available from: doi:10.1016/j.compgeo.2019.103166

A series of errors generally concerning the axes labels and legends of some of the figures included in Publication IV were detected after publication. These errors are inconsequential and do not alter at all the conclusions of this publication, but rather correction of these facilitate the reading of the paper.

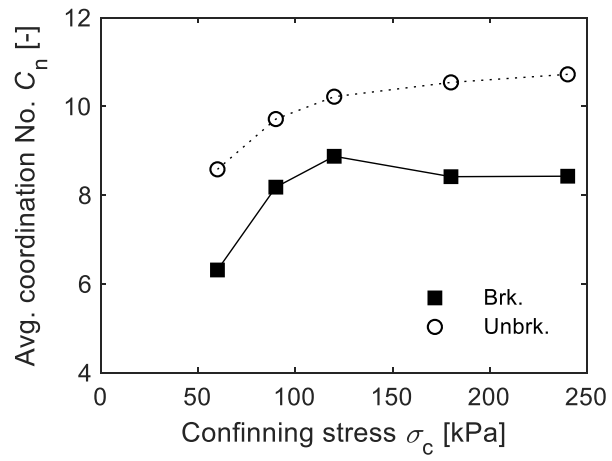
Fig. 6. Deviator stress against axial strain under cyclic triaxial loading for (a) unbreakable assemblies, (b) breakable assemblies, (c) experimental results for gradation B in [16] and (d) bonded model in [9].

- Y-axis should read “Deviator stress σ_d [kPa]” on figures 6(a), 6(b), 6(c) and 6(d).
- A legend identical to the one for Fig. 7(d) should appear on Fig. 6(d).

Fig. 7. Volumetric strain against axial strain under cyclic triaxial loading for (a) unbreakable assemblies, (b) breakable assemblies, (c) experimental results for gradation B in [16] and (d) bonded model in [9].

- Y-axis should read “Volumetric strain ε_v [-]” on figures 7(a), 7(b), 7(c) and 7(d).

A mistake in the calculation of the average coordination number C_n for the breakable tests was detected, resulting in a slight modification of Fig. 12. Effect of confinement on the final average coordination number for unbreakable and breakable triaxial test. The figure should be as follows:



None of the text in connection with Fig. 12 in the article needs to be modified.

Appended papers

TRITA-ABE-DLT-205
ISBN 978-91-7873-509-9